A top-down insular cortex circuit crucial for non-nociceptive fear learning

Junho Han,[1, 2] Boin Suh,[1, 2] and Jin-Hee Han[1, 2, *]

[1]Department of Biological Sciences

[2]KAIST Institute for the BioCentury, Korea Advanced Institute of Science and Technology, Daejeon 34141, South Korea

*Correspondence: han.jinhee@kaist.ac.kr

Abstract

Understanding how threats drive fear memory formation is crucial to understanding how organisms adapt to environments and treat threat-related disorders like PTSD. While traditional Pavlovian conditioning studies have provided valuable insights, the exclusive reliance on electric shock as a threat stimulus has limited our understanding of diverse threats. To address this, we developed a conditioning paradigm using a looming visual stimulus as an unconditioned stimulus (US) in mice and identified a distinct neural circuit for visual threat conditioning. Parabrachial CGRP neurons were necessary for both conditioning and memory retrieval. Upstream neurons in the posterior insular cortex (pIC) responded to looming stimuli, and their projections to the parabrachial nucleus (PBN) induced aversive states and drove conditioning. However, this pIC-to-PBN pathway was not required for foot-shock conditioning. These findings reveal how non-nociceptive visual stimuli can drive aversive states and fear memory formation, expanding our understanding of aversive US processing beyond traditional models.

Introduction

In dynamic environments, animals must learn to recognize sensory cues and contextual information associated with threats to generate appropriate defensive responses and enhance survival. While adaptive learning is essential, maladaptive fear memories are implicated in anxiety-related disorders, including post-traumatic stress disorder (PTSD). Thus, understanding how threats drive fear memory formation is crucial for developing effective treatments (*1*). To investigate the neural mechanisms of fear learning, Pavlovian fear conditioning has been widely used across various species, particularly rodents (*2*, *3*). In this paradigm, a neutral sensory cue (conditioned stimulus, CS) is paired with an aversive stimulus (unconditioned stimulus, US), leading to fear responses upon CS re-exposure. This model has significantly advanced our understanding of fear memory formation (*4–8*). However, research has predominantly relied on electric foot shocks as the primary US, limiting our understanding of fear learning driven by other types of threats.

In natural environments, threats are not exclusively nociceptive. Predator-associated cues, such as visual or chemical signals, elicit fear-related behaviors like freezing and escape (*9–11*). Although non-nociceptive, these stimuli can induce aversive affective states, leading to fear learning, which is critical for survival by enabling avoidance of physical harm. Previous studies have used live predators and predator odors as non-nociceptive US in rodent fear learning models (*9*, *10*), identifying key brain regions involved in odor-induced fear learning, including the basolateral amygdala (BLA) (*12*),

ventral hippocampus (vHPC) (*13*), medial amygdala (MeA) (*14*), and posterior insular cortex (pIC) (*15*). However, findings on odor-based fear conditioning are inconsistent (*16–19*), as different predator odors vary in effectiveness (*10*, *20*) and activate distinct brain regions (*18*). Additionally, odor stimuli are difficult to control precisely, complicating circuit-level investigations.

In contrast, visual threat stimuli offer precise experimental control and cross-species applicability. Rapidly looming visual stimuli have been shown to trigger immediate defensive responses in rodents (*11*, *21*), frogs (*22*), fish (*23*, *24*), primates (*25*), and humans (*26*, *27*). A pioneering study established a visual threat model in mice using an overhead looming dark disc mimicking an approaching aerial predator (*11*). Given their advantages, visual threats seem to offer an ideal framework for developing novel non-nociceptive fear learning models.

Traditionally, US pathways in fear learning have been identified using foot-shock stimuli (*8*, *28–31*). Among these, the thalamus and parabrachial nucleus (PBN) in the brainstem are recognized as key ascending nociceptive pathways. The thalamus has long been considered central to nociceptive US processing due to its widespread projections across the brain (*32–36*). However, recent evidence highlights the PBN as an essential US pathway, transmitting pain-related signals to the central nucleus of the amygdala (CeA) and other downstream regions (*37*). Han et al. demonstrated that calcitonin gene-related peptide (CGRP)-expressing neurons in the PBN ($CGRP^{PBN}$ neurons) are essential for foot-shock conditioning in mice and that optogenetic activation of $CGRP^{PBN}$-CeA pathway induces fear learning (*37*).

Interestingly, $CGRP^{PBN}$ neurons respond not only to electric shocks but also to various non-nociceptive stimuli (*38*, *39*), including visual threats, suggesting a potential role in non-nociceptive fear learning. However, whether $CGRP^{PBN}$ neurons process US signals during non-nociceptive fear learning remains unclear. Furthermore, unlike nociceptive pathways, which are known to originate from the spinal cord and periaqueductal gray (PAG) (*40–42*), the upstream sources conveying non-nociceptive input to PBN neurons remain unidentified.

Here, we developed a threat conditioning paradigm in mice using the previously established looming visual threat. Through this model, we identified PBN^{CGRP} neurons and a distinct pIC-to-PBN top-down circuit as essential for visual threat conditioning. Notably, this circuit was not required for foot-shock conditioning. Furthermore, the pIC-to-PBN circuit was sufficient to induce aversive affective states and drive threat conditioning as a US. These findings highlight its role in processing threat-relevant, non-nociceptive visual information, independent of sensory pain pathways.

Results

Looming Visual Stimuli Drive Threat Conditioning as a US

We aimed to develop a visual threat conditioning model using a looming visual stimulus as a US. The stimulus consisted of a rapidly expanding dark disc (5° to 35° visual angle in 300 ms), which remained at full size for 500 ms. First, we confirmed that this stimulus induces innate defensive responses in mice. Exposure to 10 consecutive looming stimuli elicited robust freezing, either immediately or following an escape response (**Fig. 1, A to C**). Eight animals exhibited immediate freezing, while the remaining two initially escaped before freezing. A previous study (*43*) reported predominant escape-freezing responses over immediate freezing in a no-shelter condition. However, differences in experimental conditions, particularly looming stimulus parameters, may account for these

discrepancies. Notably, another study (*44*) used looming stimuli similar to ours and reported that mice primarily exhibited immediate freezing in a no-shelter condition, consistent with our findings.

Given that looming stimuli pose no actual harm, we tested for habituation. Mice exposed to looming stimuli across five days showed no significant reduction in freezing (**fig. S1A, B**). However, when the same stimulus was repeatedly presented within short intervals (five stimuli per session, repeated 10 times with 120-s intertrial intervals [ITI]), freezing responses declined after the 7th exposure, indicating habituation (**fig. S1D, E**). This reduction in freezing was not due to a shift in defensive behavioral patterns, as repeated looming exposures did not increase escape behavior probability (**fig. S1C, F**). While significant habituation was observed after the 7th trial, some mice exhibited a decrease in freezing levels to looming stimuli relative to baseline freezing starting from the 6th trial (**fig. S1G**). Based on these findings, we used five CS-US pairings in subsequent conditioning experiments.

To determine whether looming stimuli can serve as an effective US, we paired a neutral auditory tone (2.7 kHz, 80 dB) as a CS with five consecutive looming stimuli as a US (looming US). In the paired group, the tone was presented for 20 s, overlapping with the final 4 s of the looming US. In the unpaired group, the US and CS were presented separately with a randomized 15- to 30-s interval (**Fig. 1D**). During the retrieval test in a different context, only the paired group exhibited significant freezing to the tone (**Fig. 1E**). Contextual fear memory was also assessed by re-exposing mice to the original conditioning chamber, where both groups showed significant freezing (**Fig. 1F**). Additional experiments revealed that fewer than five CS-US pairings failed to establish robust conditioning (**Fig. 1G**). These results demonstrate that a non-nociceptive visual threat can drive robust fear learning as a US in mice.

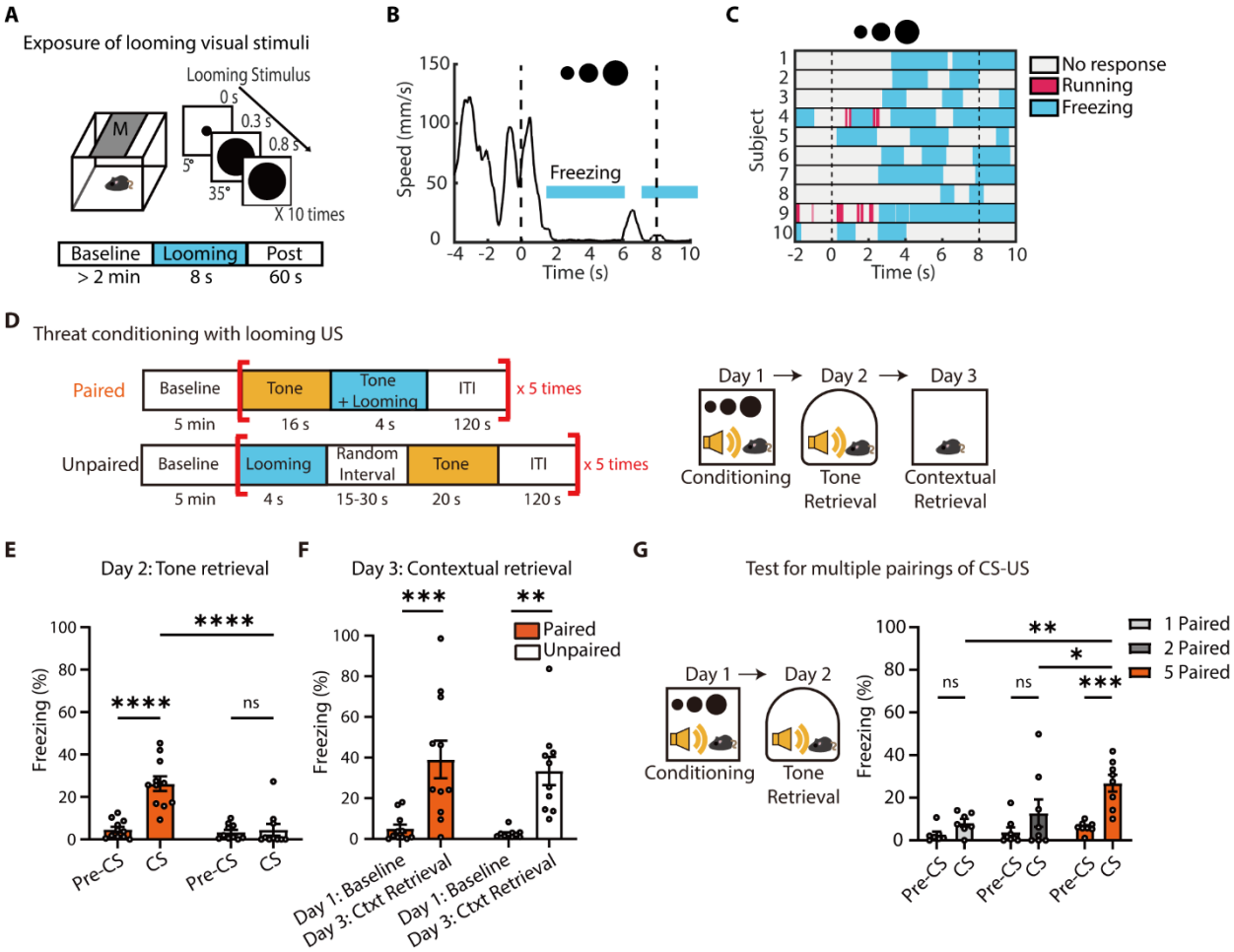

Fig. 1. Looming visual stimuli drive formation of auditory and contextual fear memory in mice

(**A**) Schematic of behavioral tests for exposure of looming visual stimuli (a 10-times repeat of a single looming for 8 s). (**B**) Changes in movement speed of mice in response to looming visual stimuli. The blue shaded bars indicate a period during which mice displayed freezing behavior. (**C**) Ethogram showing defensive behavioral responses to the presentation of looming visual stimuli. Mice displayed robust freezing, either immediately or following an escape response (N= 10, 8 mice showed immediate freezing and other 2 mice showed escape-freezing). (**D**) Schematic of a threat conditioning protocol with looming visual stimuli. (**E**) Auditory fear memory was formed only in the paired group (Paired group, N= 11; Unpaired group, N= 10; RM two-way ANOVA, Time × Group, $F_{1,19}$= 17.2, P= 0.0005). (**F**) Both paired and unpaired groups show elevated levels of contextual freezing during re-exposure to the conditioning chamber on day3 (RM two-way ANOVA, Time, $F_{1,19}$= 36.38, P< 0.0001). (**G**) Single and double pairings of tone CS and looming US were not effective in driving the formation of auditory fear memory (Single-paired group, N= 7; Double-paired group, N= 8; Five-times paired group, N= 8; RM two-way ANOVA, Group, $F_{2,20}$= 4.500, P= 0.0243; right). All data are mean ± s.e.m. *p < 0.05. **p < 0.01. ***p < 0.001. ****p < 0.0001. ns, not significant.

CGRP^{PBN} neurons selectively respond to looming US and acquired tone CS, but not to neutral stimuli.

The PBN is a major ascending nociceptive pathway with extensive connections to the CeA and hypothalamus (*45*, *46*), regulating emotional behaviors and autonomic responses. This suggests its primary role in the affective pain processing rather than sensory pain perception. Affective pain, defined as the emotional unpleasantness of pain (*47–50*), drives avoidance behavior, facilitating fear learning. Supporting this, CGRP^{PBN} neurons are essential for foot-shock conditioning, and optogenetic activation of the CGRP^{PBN}-CeA pathway induces fear memory formation (*37*). Beyond nociceptive processing, CGRP^{PBN} neurons also respond to various non-nociceptive aversive stimuli (*39*) and regulate food neophobia (*38*), suggesting a broader function in aversive state encoding. These findings indicate that the PBN serves as a general danger-detection hub (*51*), integrating diverse aversive signals and regulating emotional behaviors. Thus, we reasoned that CGRP^{PBN} neurons may also contribute to fear memory formation in response to visual threats.

First, to verify whether CGRP^{PBN} neurons specifically respond to looming visual stimuli, we performed in vivo fiber photometry calcium recordings in CGRP^{PBN} neurons during exposure to looming and flickering stimuli (a non-threatening control; **Fig. 2A**). Cre-dependent AAV encoding GCaMP6m was injected into the PBN of *Calca^{Cre}* transgenic mice (*52*), in which Cre recombinase is specifically expressed in CGRP+ neurons, with an optic fiber implanted above the injection site (**Fig. 2B**). While flickering stimuli failed to induce freezing, looming threats elicited strong freezing responses (**Fig. 2C**). Correspondingly, CGRP^{PBN} neurons exhibited no calcium activation in response to flickering stimuli but showed significant and sustained activation (~1 min) following looming threats (**Fig. 2, D to G**). These results demonstrate that CGRP^{PBN} neurons selectively respond to threatening visual stimuli rather than neutral visual cues.

Next, we examined CGRP^{PBN} activity during visual threat conditioning and tone retrieval tests. Mice were divided into paired and unpaired conditioning groups (**Fig. 2H**). As expected, both groups showed increased CGRP^{PBN} activity in response to the looming US during conditioning (**Fig. 2, I to L**). However, during retrieval, only the paired group exhibited increased calcium activity in response to the tone CS (**Fig. 2, M to O**). These findings suggest that following conditioning, CGRP^{PBN} neurons encode the acquired danger value of the tone CS, likely through synaptic plasticity-dependent mechanisms.

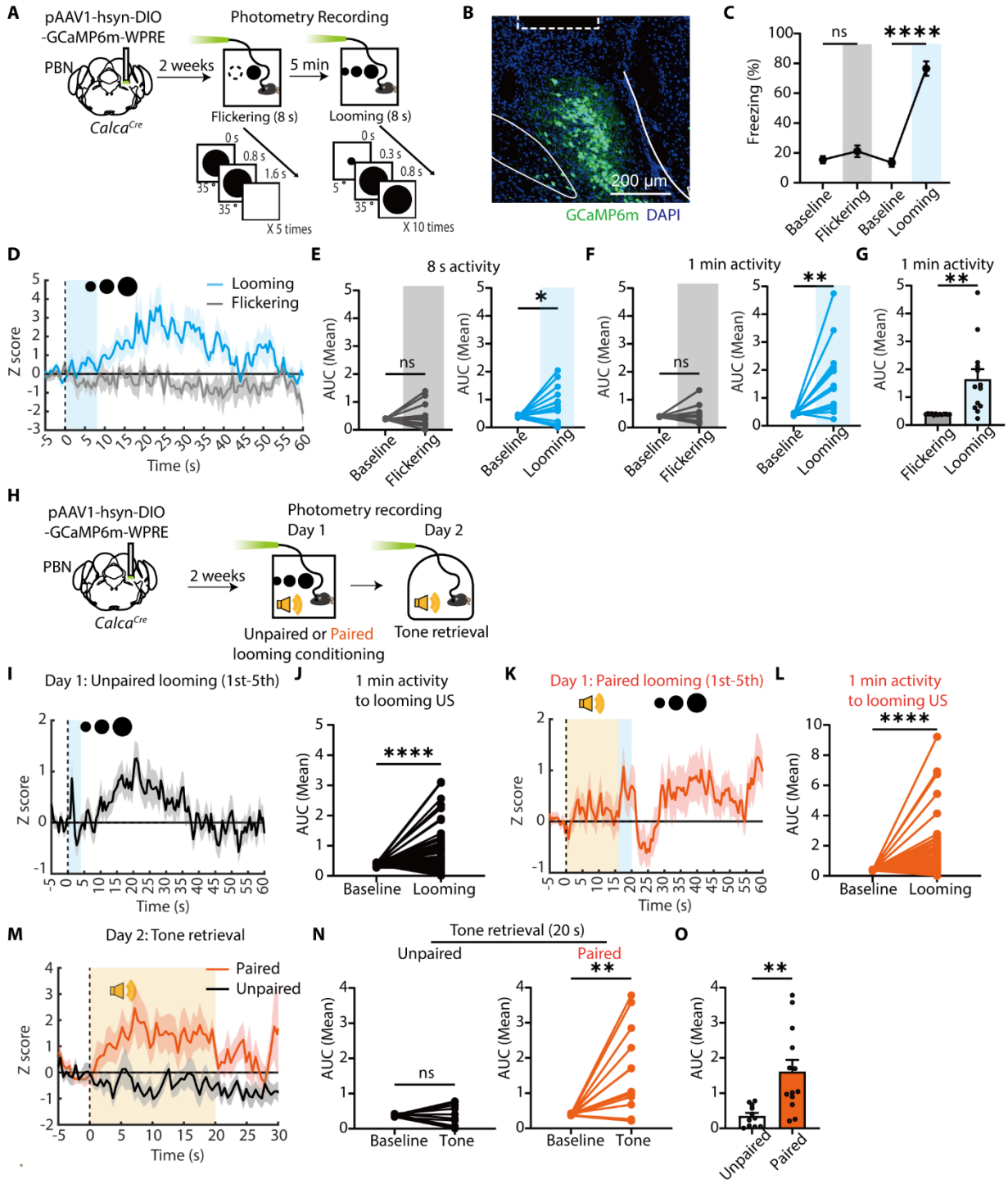

Fig. 2. CGRP^{PBN} neurons selectively respond to looming US and acquired tone CS, but not to neutral stimuli

(**A**) Schematic of fiber photometry recordings in CGRP^{PBN} neurons during visual stimuli. (**B**) Representative image of GCaMP6m expression in the PBN; the dotted rectangle marks the optic fiber location. (**C**) Freezing levels during flickering and looming stimuli (N= 13 mice; RM one-way ANOVA, Time, $F_{12,36}$= 2.786, P= 0.0087). (**D**) Z-scored calcium activity (mean ± s.e.m.) during visual stimuli. (**E, F**) Average area under the curve (AUC) comparison of calcium activity during visual stimuli (E; flickering; N= 13 mice; two-tailed paired t-test, t_{12}= 0.6077, P= 0.5547; looming; t_{12}= 2.221, P= 0.0464) and during 1 min (F; flickering; t_{12}= 0.6251, P= 0.5436; looming; t_{12}= 3.482, P= 0.0045). (**G**) AUC comparison between flickering and looming stimuli (t_{12}= 3.541, P= 0.0041). (**H**) Schematic of fiber photometry recordings of CGRP^{PBN} neurons

during visual threat conditioning. (**I-J**) Z-scored calcium activity of $CGRP^{PBN}$ neurons in the unpaired group during the 1st-5th exposures to looming US (J; *N*= 55 trials; two-tailed Wilcoxon matched-pairs signed rank test, W= -1042, *P*< 0.0001). (**K-L**) Z-scored calcium activity of $CGRP^{PBN}$ neurons in the paired group during the 1st-5th exposures to looming US (L; N = 65 trials; two-tailed Wilcoxon matched-pairs signed-rank test, W = -1261, *P* < 0.0001). (**M**) Z-scored calcium activity of $CGRP^{PBN}$ neurons during the tone retrieval test. (**N**) Average AUC of calcium activity in the unpaired (left; two-tailed paired t-test, t_{10}= 0.3602, *P*= 0.7262) and paired groups (right; t_{12}= 3.714, *P*= 0.0030) during the tone retrieval test. (**O**) Comparison of AUC between the two groups during the tone retrieval test (Two-tailed unpaired t-test, t_{22}= 3.431, *P*= 0.0024). All data are mean ± s.e.m. *p < 0.05. **p < 0.01. ****p < 0.0001. ns, not significant.

$CGRP^{PBN}$ neurons are required for fear memory formation and its retrieval, but not for innate defensive response to a visual threat

To assess the necessity of $CGRP^{PBN}$ neurons in visual threat conditioning, we inactivated them using tetanus toxin light chain (TetTox)(*53*). Cre-dependent AAV encoding TetTox and dTomato was injected into the PBN of $Calca^{Cre}$ mice, with tdTomato alone serving as a control (**Fig. 3A**). Post hoc histological analysis confirmed restricted viral expression in the PBN (**Fig. 3B**). Open-field tests confirmed no locomotor or anxiety differences between groups before conditioning (**Fig. 3C**).

During conditioning, both TetTox and control groups exhibited similar freezing to the looming US (first CS-US pairing), indicating that $CGRP^{PBN}$ neurons are not essential for innate defensive responses to visual threats (**Fig. 3D**), consistent with prior studies (*39*). This finding was further validated in an independent experiment (**fig. S2, A and B**). However, fear memory formation was significantly impaired—TetTox-expressing mice showed no significant increase in freezing to the conditioned tone or context, whereas control mice exhibited robust freezing (**Fig. 3, E and F**). This suggests that $CGRP^{PBN}$ neurons are required for fear learning but not for reflexive defensive behaviors to looming stimuli.

To further investigate the role of $CGRP^{PBN}$ neurons in visual threat conditioning and memory retrieval, we performed optogenetic inhibition. Cre-dependent AAV encoding eNpHR3.0-EYFP or EYFP alone was injected into the PBN of $Calca^{Cre}$ mice, with an optic fiber implanted above the injection site. Light delivery inactivated $CGRP^{PBN}$ neurons throughout conditioning, beginning at the onset of the first US presentation and continuing until the session concluded (**Fig. 3G**). Histological analysis confirmed highly restricted eNpHR3.0 expression in the PBN (**Fig. 3H**).

Consistent with the TetTox experiment, immediate freezing responses (measured during first CS-US pairing) were unaffected (**Fig. 3I**). However, fear memory formation was abolished in the eNpHR3.0 group (**Fig. 3J**). In a separate experiment, inhibition of $CGRP^{PBN}$ neurons during retrieval, rather than conditioning, resulted in significantly impaired freezing to the tone CS, indicating a role in memory retrieval (**Fig. 3, K and L**). Together, these findings demonstrate that $CGRP^{PBN}$ neurons are required for fear memory formation and retrieval but are dispensable for innate defensive responses to visual threats.

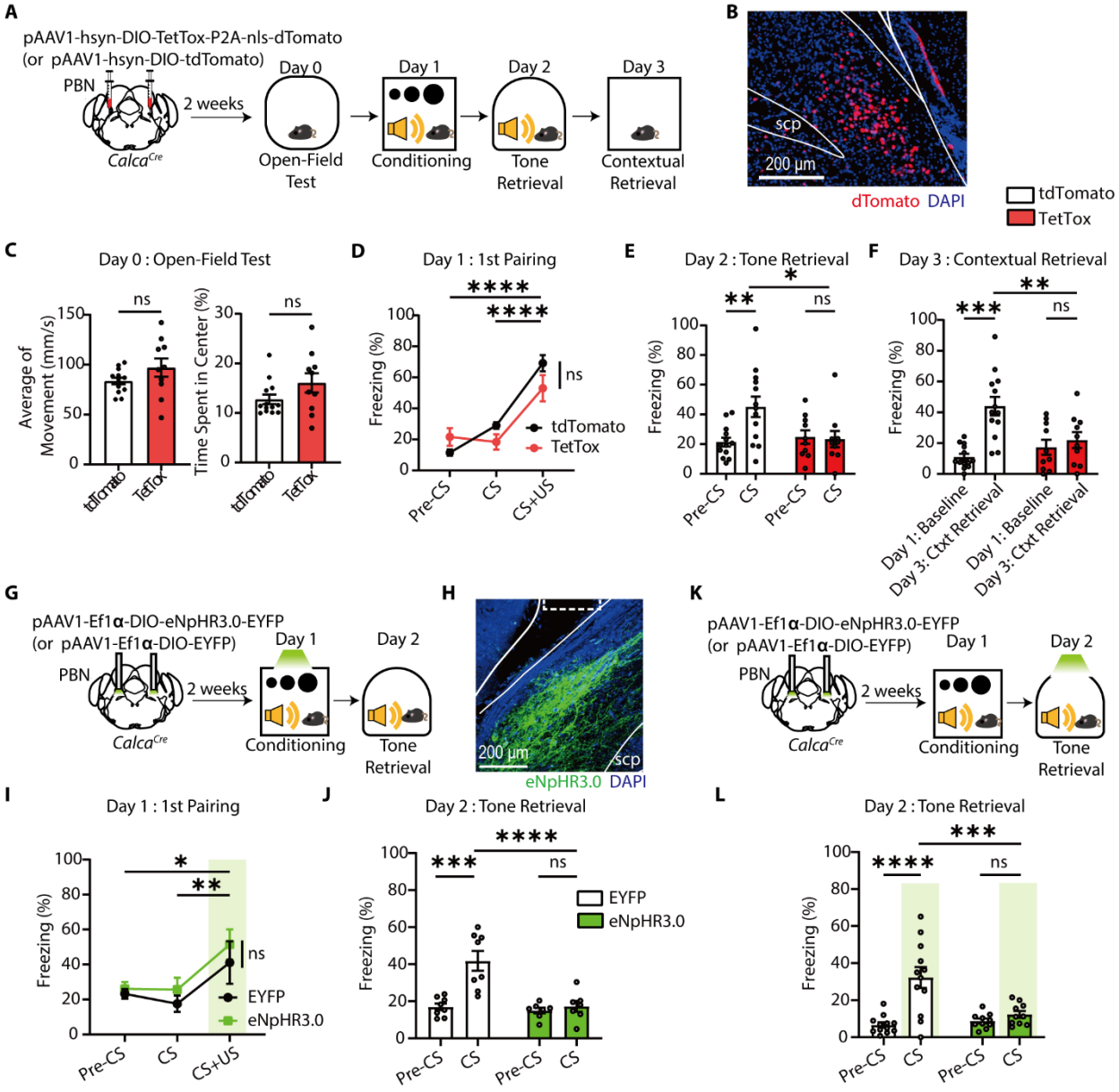

Fig. 3. The inhibition of CGRP^{PBN} neurons impairs fear memory formation and retrieval but not innate defensive behavior to looming stimuli

(**A**) Schematic of TetTox-mediated inhibition of CGRP^{PBN} neurons during visual threat conditioning. (**B**) Representative image showing the expression of dTomato in the PBN, especially in the external lateral subdivision of PBN (PBel). Scale bars, 200 µm. SCP, superior cerebellar peduncle. (**C**) Average of movement (left; TetTox, N= 10; tdTomato, N = 13; two-tailed unpaired t-test, t_{21}= 1.518, P= 0.1439) and center zone time (right, two-tailed Mann Whitney test, U= 46, P= 0.2569) were comparable between groups. (**D**) Freezing levels during the first CS–US pairing on Day 1 (RM two-way ANOVA, Time × Group, $F_{2,42}$= 5.334, P= 0.0086). (**E-F**) TetTox inhibition of CGRP^{PBN} neurons impairs auditory (E; RM two-way ANOVA, Time × Group, $F_{1,21}$= 7.251, P= 0.0136) and contextual fear memory (F; RM two-way ANOVA, Time × Group, $F_{1,21}$= 7.798, P= 0.0109). (**G**) Schematic of optogenetic inhibition of CGRP^{PBN} neurons during visual threat conditioning. (**H**) Representative image of eNpHR3.0-EYFP expression in CGRP^{PBN} neurons; the dotted rectangle marks the optic fiber tip location. Scale bars, 200 µm. (**I**) Freezing during the first CS–US pairing (eNpHR3.0, N= 7; EYFP, N= 8; RM two-way ANOVA, Time, $F_{2,26}$= 7.167, P= 0.0033). (**J**) Inhibition of CGRP^{PBN} neurons

during visual US conditioning impaired the formation of auditory fear memory (RM two-way ANOVA, Time × Group, $F_{1,13}$= 9.965, P= 0.0076). (**K**) Schematic of optogenetic inhibition of $CGRP^{PBN}$ neurons during auditory memory retrieval. (**L**) Inhibition of $CGRP^{PBN}$ neurons impaired retrieval of auditory fear memory (eNpHR3.0, N= 10; EYFP, N= 12; RM two-way ANOVA, Time × Group, $F_{1,20}$= 18.16, P= 0.0004). All data are mean ± s.e.m. *p < 0.05. **p < 0.01. ***p < 0.001. ****p < 0.0001. ns, not significant.

pIC and SC cells projecting to the $CGRP^{PBN}$ neurons are activated by looming visual stimuli

$CGRP^{PBN}$ neurons are critical for visual threat conditioning, but their upstream non-nociceptive inputs remain unclear. While nociceptive stimuli are relayed via the spinal cord or PAG (*37*, *40–42*), the pathway conveying non-nociceptive US information is less understood. To identify $CGRP^{PBN}$ inputs, we performed monosynaptic retrograde tracing by injecting Cre-dependent AAV-hsyn-DIO-TVA-HA-N2cG into the PBN of *Calca*^{Cre} mice, followed by SADB19-GFP rabies virus (**fig. S3A**). Starter cells were localized exclusively in the PBN (**fig. S3B**), and retrogradely labeled neurons were observed in ipsilateral and contralateral brain regions associated with emotional processing, sensory integration, and motor functions, including the pIC, CeA, PAG, and superior colliculus (SC) (**fig. S3, C to E**).

To determine which of these inputs are activated by visual threats, we analyzed c-Fos expression in projection neurons following looming or flickering stimuli. Mice injected bilaterally with AAV helper and rabies virus were exposed to either looming or flickering stimuli (**Fig. 4A, fig. S4A**). Only looming stimuli significantly increased freezing behavior (**Fig. 4B**). We analyzed c-Fos expression in fear- and vision-related upstream regions, including the insular cortex (IC), CeA, PAG, and SC. Anatomically, $CGRP^{PBN}$-projecting neurons were identified in both the anterior (aIC) and posterior IC (pIC) in layers 5 and 6 (**fig. S5, B and C**), but projections from the pIC were notably denser (**fig. S5D**). Given that the pIC is more closely associated with pain and aversive states, whereas the aIC is primarily linked to appetitive processing (*54–56*), we focused on the pIC as a key candidate for relaying aversive affective signals. In the pIC, most GFP+ cells showed significantly greater activation in the looming group than in the flickering group (**Fig. 4C, D, and fig. S5A, B**). Similarly, SC GFP+ neurons in the intermediate layers exhibited significantly increased activation to looming (**Fig. 4, C, G**). This pIC and SC-specific activation was restricted to GFP+ projection neurons, as no group differences were found in GFP- populations across brain regions (**Fig. 4, C to G**). In contrast, no activation differences were observed in the CeA or PAG (**Fig. 4, C, E, and F**). These findings suggest that projection neurons in the pIC ($pIC^{\rightarrow CGRP\text{-}PBN}$) and SC are selectively activated by looming threats and may serve as upstream sources of US information for $CGRP^{PBN}$ neurons.

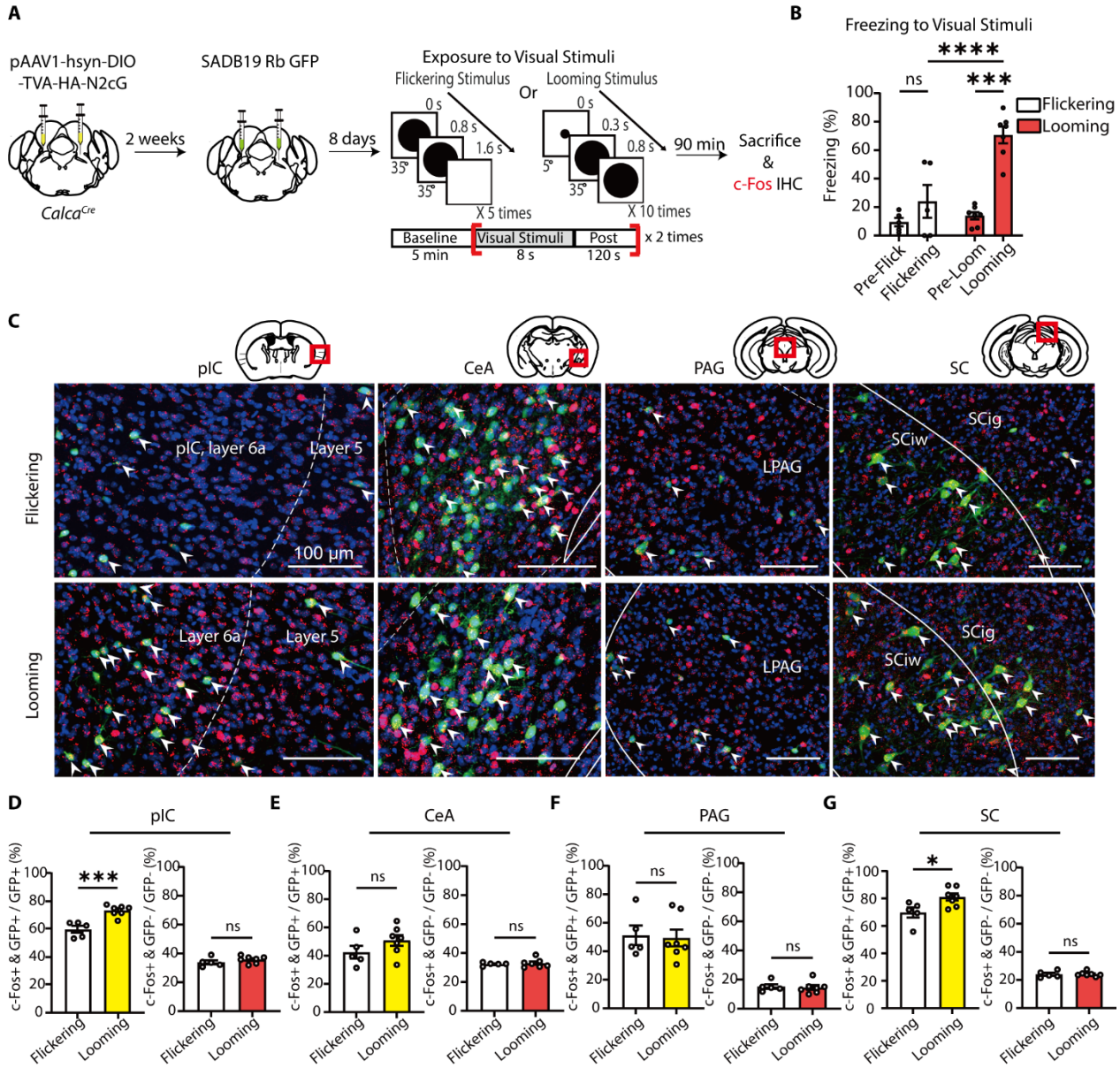

Fig. 4. Identification of CGRP^{PBN}-projecting neurons activated by looming visual stimuli

(**A**) Schematic of a monosynaptic retrograde tracing of CGRP^{PBN} neurons and c-Fos imaging in response to looming stimuli. Bilateral injections of AAV2/1-hsyn-DIO-TVA-HA-N2cG into the PBN of *Calca*^{Cre} mice were followed by bilateral injections of SADB19-GFP rabies virus into the same site. (**B**) Looming visual stimuli induced a robust freezing response in mice, whereas flickering stimuli did not (Flickering, N= 5, Looming, N= 7; RM two-way ANOVA, Time × Group, $F_{1,10}$= 9.893, P= 0.0104). (**C**) Representative confocal microscopic images showing CGRP^{PBN}-projecting GFP+ neurons (Green) and c-Fos+ neurons (Red) in the pIC, CeA, PAG, and SC. A white arrowhead indicates co-localized neurons. Images of starter cells in the PBN are presented in the fig. S4. Scale bars, 100 µm. LPAG, lateral periaqueductal gray; SCiw, intermediate white layer of the superior colliculus; SCig, intermediate gray layer of the superior colliculus. (**D-G**) The ratio of double-positive neurons (GFP+ & c-Fos+) within GFP+ or GFP- cell populations was compared between the groups (Flickering vs Looming) in each analyzed region: pIC (D) (Flickering, N= 5; Looming, N= 7; left; Two-tailed unpaired t-test, t_{10}= 4.952, P= 0.0006; right; t_{10}= 1.145, P= 0.2787), CeA (E) (left; t_{10}= 1.404, P = 0.1906; right; t_{10}= 0.4580, P= 0.6567), PAG (F) (left; t_{10}= 0.2072, P = 0.8400; right; t_{10}= 0.2809, P= 0.7845), and SC (G) (left;

t_{10}= 2.593, P= 0.0268; right; t_{10}= 0.1301, P= 0.8901). All data are mean ± s.e.m. *p < 0.05. ***p < 0.001. ****p < 0.0001. ns, not significant.

Selective activation of pIC$^{\rightarrow CGRP\text{-}PBN}$ neurons in response to threat stimuli

The IC is well known for processing negative emotions and contributing to fear, anxiety, and disgust (*48*, *57*). In humans, IC activity correlates with affective and social pain, and lesions can lead to pain asymbolia, where pain is perceived without emotional distress (*48*, *58–60*). In rodents, optogenetic activation of the pIC induces an aversive state (*56*), and pIC activity is required for maintaining learned fear (*61*), suggesting its role in encoding aversive affect rather than sensory pain.

The IC has also been implicated in non-nociceptive fear conditioning. In humans, exposure to aversive images as a US increases IC activation in response to both the US and CS (*62*, *63*). In rodents, inactivation of the pIC impairs predator odor fear conditioning and memory recall (*15*). Notably, the IC has extensive reciprocal connections with the PBN (*45*, *46*), and we identified the increased activity of pIC$^{\rightarrow CGRP\text{-}PBN}$ neurons in response to looming stimuli (**Fig. 4D**). Based on these findings, we hypothesized that the pIC transmits threat-relevant aversive affective signals to the CGRP^{PBN} neurons to drive visual threat conditioning.

To further prove whether pIC$^{\rightarrow CGRP\text{-}PBN}$ neurons selectively respond to threat stimuli, we performed photometry calcium recordings. Using a rabies-virus-based Flp system, we expressed GCaMP6s selectively in pIC$^{\rightarrow CGRP\text{-}PBN}$ neurons (**Fig. 5, A–C**). Mice were exposed to either looming and foot shock stimuli or flickering and foot shock stimuli. Photometry recordings revealed that pIC$^{\rightarrow CGRP\text{-}PBN}$ neurons were persistently activated by both looming and foot shock stimuli but exhibited distinct activation dynamics: a slow increase to looming and a rapid increase to foot shock (**Fig. 5, D–F**). In contrast, flickering stimuli did not induce pIC$^{\rightarrow CGRP\text{-}PBN}$ activation, whereas foot shock elicited a robust response (**Fig. 5, G–I**). These findings indicate that pIC$^{\rightarrow CGRP\text{-}PBN}$ neurons selectively respond to threats rather than general sensory stimuli.

Moreover, the sustained activity of pIC$^{\rightarrow CGRP\text{-}PBN}$ neurons beyond threat exposure suggests they encode persistent aversive states rather than transient threat detection (*56*, *64*, *65*). Their prolonged response to looming stimuli also parallels the sustained activation observed in CGRP^{PBN} neurons (**Fig. 2D**), suggesting that pIC input may contribute to prolonged CGRP^{PBN} activation.

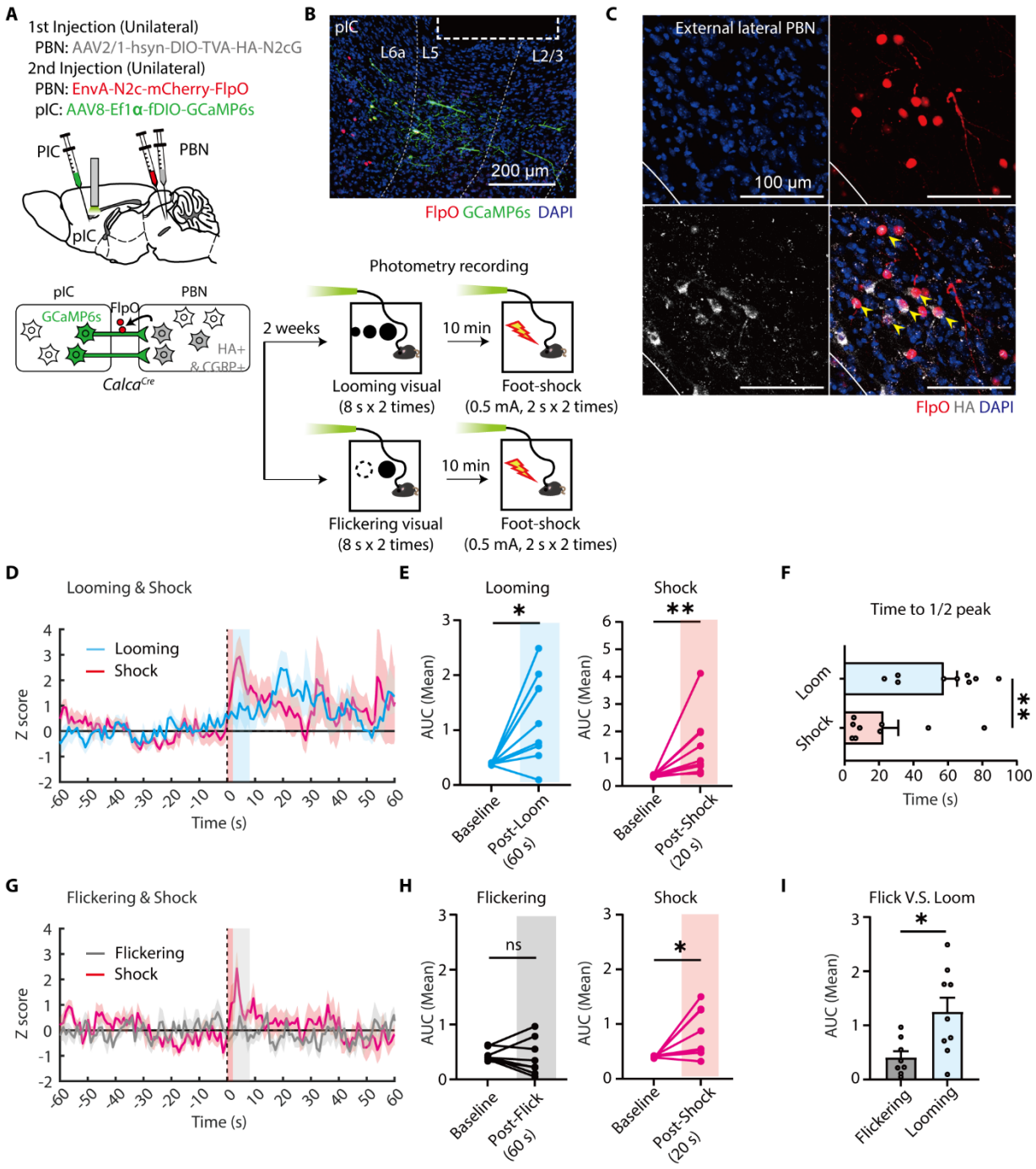

Fig. 5. Fiber photometry recordings of pIC$^{\rightarrow CGRP\text{-}PBN}$ neuronal activity in response to visual and foot-shock stimuli.

(A) Schematic of fiber photometry recordings of pIC$^{\rightarrow CGRP\text{-}PBN}$ neuronal responses to looming (or flickering) & foot-shock stimuli. **(B)** Representative image of GCaMP6s (green) and FlpO (red) expression in the pIC. All GCaMP6s+ cells were FlpO+. The dotted rectangle marks the optic fiber location. Scale bar, 200 µm. **(C)** Representative images of starter cells in the PBN. Yellow arrowheads indicate FlpO-mCherry+ & HA+ starter cells. Scale bars, 100 µm. **(D)** Z-scored calcium activity (mean ± s.e.m) in response to looming and foot-shock stimuli (the blue shaded area: 8-s looming stimuli; the red shaded area: 2-s foot-shock). **(E)** Average during looming and foot-shock (*N*= 9 mice; left; baseline = -60 to 0 s, looming = 0-60 s after the onset of visual stimuli; Two-tailed paired t-test, t_8= 3.291, *P*= 0.011; right; shock = 0-20 s after the onset of shock stimuli; Two-tailed Wilcoxon matched-pairs signed rank test, W= 45, *P*= 0.0039). **(F)** Time

345 to reach half of the peak z-score after the peak (Two-tailed Mann Whitney test, U= 11, *P*=
346 0.0072). **(G)** Z-scored calcium activity (mean ± s.e.m) during flickering and foot-shock (the gray
347 shaded area: 8-s flickering stimuli; the red shaded area: 2-s foot-shock). **(H)** Average AUC during
348 flickering and foot-shock (*N*= 8 mice; left; baseline = -60 to 0 s, flickering = 0-60 s after the onset
349 of visual stimuli; Two-tailed Wilcoxon matched-pairs signed rank test, W= -6, *P*= 0.7422; right;
350 shock = 0-20 s after the onset of shock stimuli; Two-tailed paired t-test, t_7= 2.791, *P*= 0.0269). **(I)**
351 Comparison of AUC between flickering and looming (Two-tailed unpaired t-test, t_{15}= 2.798, *P*=
352 0.0135). All data are presented as mean ± s.e.m. *p < 0.05, **p < 0.01; ns, not significant.

353

354 **pIC$^{\rightarrow PBN}$ neurons are required for CGRP^{PBN} neuronal activation by visual threats**
355 **but not to foot shock**

356 If the pIC transmits threat-relevant signals to CGRP^{PBN} neurons, then its input
357 should be required for CGRP^{PBN} activation. To test this, we inhibited pIC neurons
358 projecting to the PBN (pIC$^{\rightarrow PBN}$) using DREADDs (Designer Receptors Exclusively
359 Activated by Designer Drugs) while monitoring CGRP^{PBN} activity in response to looming
360 and foot shock. Cre-dependent AAV-hsyn-DIO-GCaMP6m was injected into the PBN of
361 *Calca^{Cre}* mice, and an optic fiber was implanted above the injection site (**Fig. 6A**). To
362 selectively express hM4Di DREADDs in pIC$^{\rightarrow PBN}$ neurons, AAVretro-FlpO was injected
363 into the PBN, followed by Flp-dependent AAV encoding hM4Di-mCherry (or mCherry as
364 a control) into the pIC (**Fig. 6B**).

365 Compound 21 (C21), a DREADD agonist (*66*), was administered 1 hour before
366 photometry recordings to inhibit pIC$^{\rightarrow PBN}$ neurons. In response to looming stimuli,
367 CGRP^{PBN} activation was significantly reduced in the hM4Di group compared to controls
368 (**Fig. 6, C to F**), with a persistent suppression lasting over 1 min (**Fig. 6 G**). By contrast,
369 CGRP^{PBN} neurons in the hM4Di group responded normally to foot shock (**Fig. 6, H–L**).
370 These findings indicate that pIC input is required for looming-induced CGRP^{PBN}
371 activation but not for foot-shock responses. Given the pIC's primary role in processing
372 aversive affect, the absence of pIC$^{\rightarrow PBN}$ input during foot shock may be compensated by
373 alternative nociceptive pathways, such as those involving the spinal cord or PAG.

374 Further axon tracing of pIC$^{\rightarrow PBN}$ neurons (**fig. S6**) revealed projections to multiple
375 brain regions, including the CeA, Basomedial amygdalar nucleus (BMA),
376 Parasubthalamic nucleus (PSTN), posterior thalamic regions, and PAG—key areas in
377 emotional regulation and learning (*39*, *67–70*). This suggests that pIC$^{\rightarrow PBN}$ neurons encode
378 aversive states and broadly relay this information to coordinate behavioral and
379 physiological responses. The observed collateral projections imply that pIC$^{\rightarrow PBN}$ input
380 contributing to CGRP^{PBN} neuronal responses to looming stimuli may be relayed either
381 directly or indirectly through other regions.

382

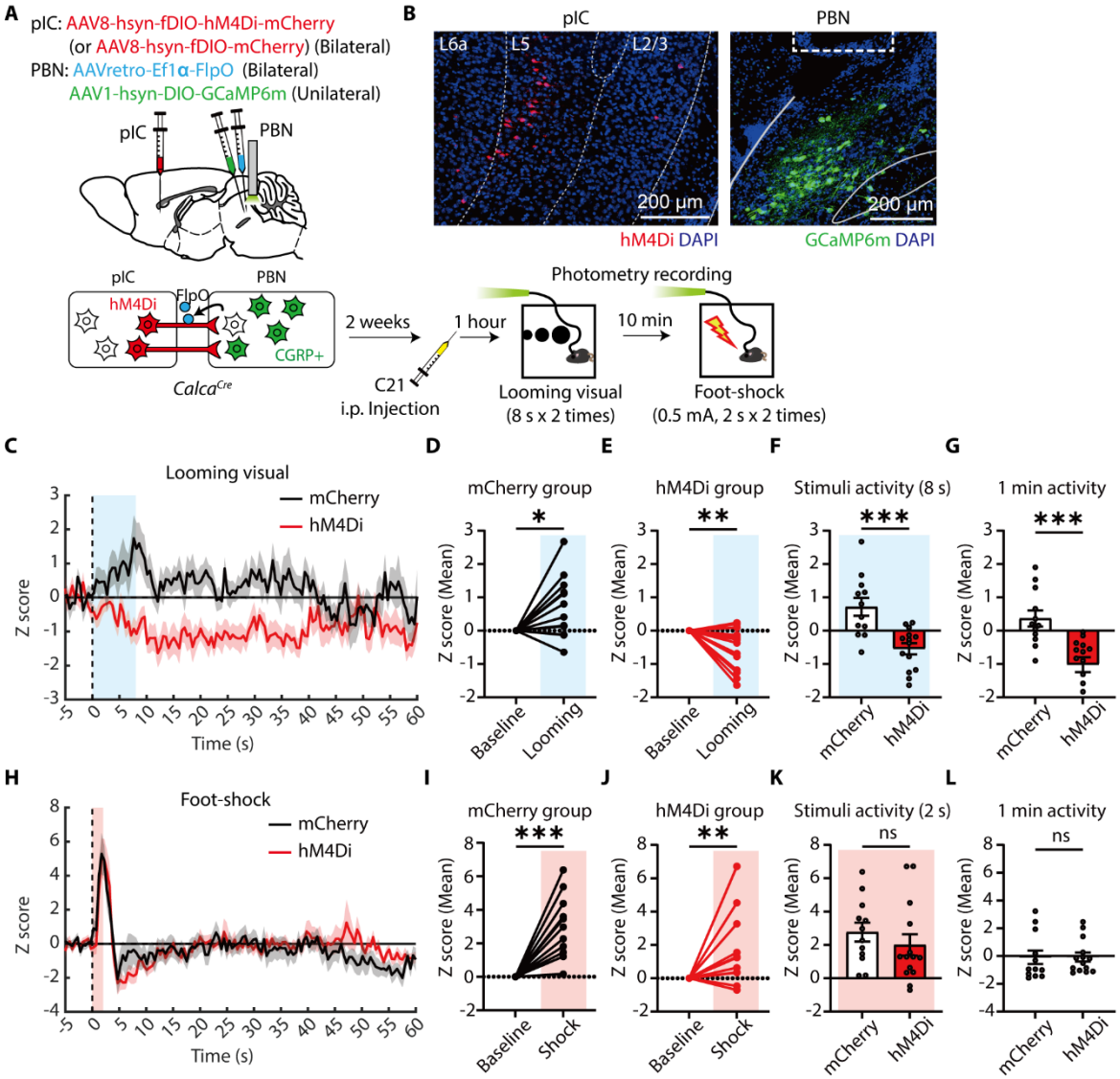

383

384 **Fig. 6. pIC$^{\rightarrow PBN}$ neurons are necessary for activation of CGRP^{PBN} neurons to looming but**
385 **not foot-shock stimuli**

386 (**A**) Schematic of photometry recording of CGRP^{PBN} neurons with hM4Di inhibition of pIC$^{\rightarrow PBN}$
387 neurons. (**B**) Representative images showing expression of hM4Di-mCherry in the pIC$^{\rightarrow PBN}$
388 neurons (left) and GCaMP6m in CGRP^{PBN} neurons (right). The dotted rectangle indicates the
389 location of optic fiber. Scale bar, 200 μm. (**C**) Z-scored calcium activities of CGRP^{PBN} neurons to
390 visual stimuli (blue shaded area: 8-s looming stimuli). (**D-E**) Average calcium activity during
391 visual stimuli in the mCherry group (D) (baseline = −5 to 0 s, looming = 0 to 8 s; N=12 trials; 2
392 trials per mouse, 6 mice; one sample t-test, t_{11}= 2.659, P= 0.0222) and hM4Di group (E) (N =14
393 trials; 2 trials per mouse, 7 mice; t_{13}= 3.266, P= 0.0061). (**F-G**) Comparison of average changes
394 in calcium activity evoked by looming stimuli between two groups during stimuli (F) (Two-tailed
395 unpaired t-test, t_{24}= 4.104, P= 0.0004) and for 1min (G) (Two-tailed unpaired t-test, t_{24}= 4.203,
396 P= 0.0003). (**H**) Z-scored calcium activities of CGRP^{PBN} neurons to foot-shock stimuli (red
397 shaded area: 2-s foot-shock). (**I-J**) Average calcium activity during foot-shock in the mCherry
398 group (I) (baseline= −5 to 0 s, shock= 0 to 2 s; N =12 trials; one sample t-test, t_{11}= 4.887, P=
399 0.0005) and hM4Di group (J) (N =14 trials; one sample Wilcoxon test, W= 89, P= 0.0031). (**K-L**)
400 Comparison of average changes in calcium activity evoked by foot-shock stimuli between two
401 groups during stimuli (K) (Two-tailed Mann Whitney test, U= 63, P= 0.2972) and for 1 min (L)

402 (Two-tailed Mann Whitney test, U= 69, *P*= 0.4624). All data are mean ± s.e.m. *p < 0.05, **p <
403 0.01. ***p < 0.001. ns, not significant.

404

405 **pIC-to-PBN pathway is necessary for visual threat conditioning but not for foot-**
406 **shock conditioning**

407 Since pIC$^{\rightarrow PBN}$ neurons are essential for CGRP^{PBN} activation by visual threats, we
408 tested whether the direct pIC-to-PBN pathway is required for visual threat conditioning.
409 To inhibit this pathway during conditioning, we injected AAV encoding eNpHR3.0-EYFP
410 (or EGFP as a control) into the bilateral pIC and implanted optic fibers above the PBN
411 (**Fig. 7, A and B**). Optogenetic inhibition during visual threat conditioning did not alter
412 immediate freezing but impaired fear memory formation (**Fig. 7, C and D**). While control
413 mice exhibited significantly increased freezing to the tone CS during retrieval, eNpHR3.0-
414 expressing mice showed no significant increase.

415 Next, we examined whether the pIC-PBN pathway is necessary for foot-shock
416 conditioning. For foot-shock conditioning, a 20-s tone CS was presented, with the last 2 s
417 paired with a 0.5-mA foot shock (**Fig. 7, E and F**). This tone-shock pairing was repeated
418 five times while inhibiting pIC-PBN terminals during conditioning. Optogenetic inhibition
419 did not affect defensive escape behavior elicited by the foot shock (**Fig. 7G**). However,
420 unlike visual threat conditioning, inhibition of pIC-PBN pathway had no effect on foot-
421 shock conditioning (**Fig. 7H**). These results indicate that the pIC-PBN pathway serves as a
422 selective US pathway for visual threat conditioning rather than foot-shock conditioning.

423 Finally, given the sustained responses of both pIC and CGRP^{PBN} neurons to
424 looming stimuli, we investigated the precise timing at which pIC input is required for
425 visual threat conditioning. We selectively inhibited the pIC→PBN pathway either strictly
426 during US exposure or during the ITI (**Fig. 7, I and J**). Inhibition during US exposure had
427 no effect on conditioned freezing (**Fig. 7I**). However, inhibition during the ITI impaired
428 fear memory formation—control mice exhibited increased freezing to the tone CS,
429 whereas eNpHR3.0-expressing mice did not (**Fig. 7J**). These results show that sustained
430 pIC→PBN input is critical for visual threat conditioning, while transient input during US
431 exposure alone is insufficient.

432 Overall, these findings suggest that pIC neurons provide essential, persistent input
433 to the PBN for visual threat conditioning but are not required for foot-shock conditioning,
434 consistent with our photometry results (**Fig. 6**).

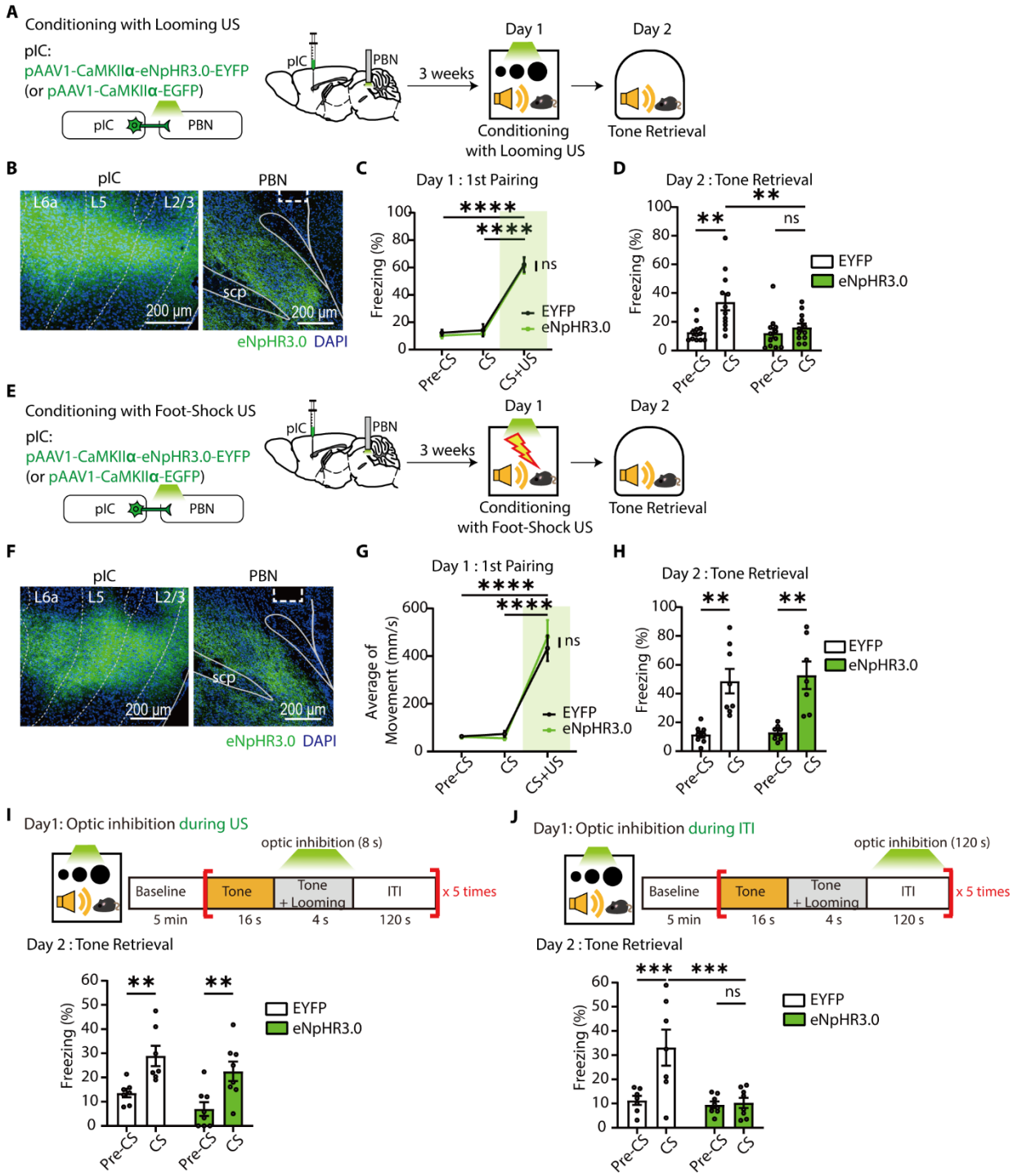

Fig. 7. pIC projections to the PBN are required for threat conditioning with looming but not with foot-shock stimuli

(**A**) Schematic of optogenetic inhibition of pIC-PBN circuit during visual threat conditioning. (**B**) Representative images of eNpHR3.0-EYFP expression in pIC neurons (left) and their axon fibers in the PBN (right). The dotted rectangle marks the optic fiber tip. Scale bars, 200 μm. (**C**) Freezing levels during the first CS-US pairing (EYFP, N= 12; eNpHR3.0, N =12; RM two-way ANOVA, Time, $F_{2,44}$= 125.6, P< 0.0001). (**D**) Optic inhibition of pIC axon terminals in the PBN during conditioning impaired auditory fear memory formation (RM two-way ANOVA, Time × Group, $F_{1,22}$= 4.550, P= 0.0443). (**E**) Schematic of optogenetic inhibition of pIC-PBN circuit during foot-shock conditioning. (**F**) Representative images of eNpHR3.0 expression in pIC

446 neurons (left) and their axon fibers in the PBN (right). The dotted rectangle marks the optic fiber
447 tip. Scale bars, 200 μm. (**G**) Average of movement during the first pairing of tone CS and foot-
448 shock US on Day 1 (EYFP, $N = 8$; eNpHR3.0, $N = 7$; RM two-way ANOVA, Time, $F_{2,26} = 71.34$,
449 $P < 0.0001$). (**H**) Optic inhibition of pIC axon terminals in the PBN during foot-shock
450 conditioning did not affect the formation of fear memory (RM two-way ANOVA, Time, $F_{1,13} =$
451 30.91, $P < 0.0001$). (**I**) Optogenetic inhibition of pIC axon terminals in the PBN during US
452 exposure did not impair auditory fear memory formation (EYFP, $N = 7$; eNpHR3.0, $N = 8$; RM
453 two-way ANOVA, Time, $F_{1,13} = 38.2$, $P < 0.0001$). (**J**) Optogenetic inhibition of pIC axon
454 terminals in the PBN during ITI impaired auditory fear memory formation (EYFP, $N = 7$;
455 eNpHR3.0, $N = 8$; RM two-way ANOVA, Time × Group, $F_{1,13} = 12.76$, $P = 0.0034$). All data are
456 mean ± s.e.m. **p < 0.01. ***p < 0.001. ****p < 0.0001. ns, not significant.

457

458 **pIC$^{\rightarrow CGRP\text{-}PBN}$ projections to the PBN induce aversive behavioral states and drive**
459 **threat conditioning as a US**

460 Our data indicate that the pIC-to-PBN circuit functions as a US pathway for visual
461 threat conditioning. As we hypothesized that this pathway transmits aversive affective
462 information, we examined whether direct activation of the circuit induces aversive
463 affective states and is sufficient to drive threat conditioning. For this purpose, we targeted
464 pIC$^{\rightarrow CGRP\text{-}PBN}$ neurons with channelrhodopsin-2 (ChR2) and optically stimulated their
465 axon terminals in the PBN (**Fig. 8A**). Cre-dependent AAV was injected into the bilateral
466 PBN of *Calca^{Cre}* mice, and Flp-dependent AAV encoding ChR2-EYFP (or EYFP alone)
467 was injected into the bilateral pIC. Two weeks later, rabies virus encoding Flp
468 recombinase fused with mCherry was injected into the PBN at the same viral injection
469 sites. Post hoc histological analysis confirmed specific ChR2 expression in pIC neurons,
470 co-expressed with Flp-mCherry (**Fig. 8B**). Starter cells were detected exclusively in the
471 PBN (**fig. S4B**). To assess aversive behaviors, we conducted the real-time place avoidance
472 (RTPA), open-field test (OFT), and elevated plus maze (EPM) tests.

473 In the RTPA test, mice were placed in a three-chamber arena where one side was
474 paired with photostimulation of pIC$^{\rightarrow CGRP\text{-}PBN}$ axon terminals in the PBN. The EYFP
475 control group showed no preference between chambers, whereas the ChR2 group avoided
476 the light-paired chamber (**Fig. 8, C to F**). In the OFT, photostimulation was alternated
477 with 60-s intervals (**Fig. 8, G and H**). The ChR2 group did not exhibit increased freezing,
478 suggesting that pIC$^{\rightarrow CGRP\text{-}PBN}$ activation does not induce freezing behavior (**Fig. 8, H and**
479 **I**). However, ChR2 mice showed increased anxiety, spending less time in the center zone
480 and crossing it fewer times than controls, despite similar total movement distance (**Fig. 8,**
481 **J to L**). In the EPM test, light stimulation was alternated (2 s on, 2 s off) throughout the
482 trial. ChR2 group spent more time in the closed arms compared to EYFP controls (**Fig.**
483 **8O**). Although not statistically significant, they also showed a tendency to spend less time
484 in the open arms (**Fig. 8N**). Additionally, the number of open arm entries was significantly
485 decreased in the ChR2 group (**Fig. 8P**), while total movement distance remained
486 comparable between groups (**Fig. 8R**). These results suggest that activation of pIC$^{\rightarrow CGRP\text{-}}$
487 ^{PBN} projections in the PBN induces aversive affective behavioral states.

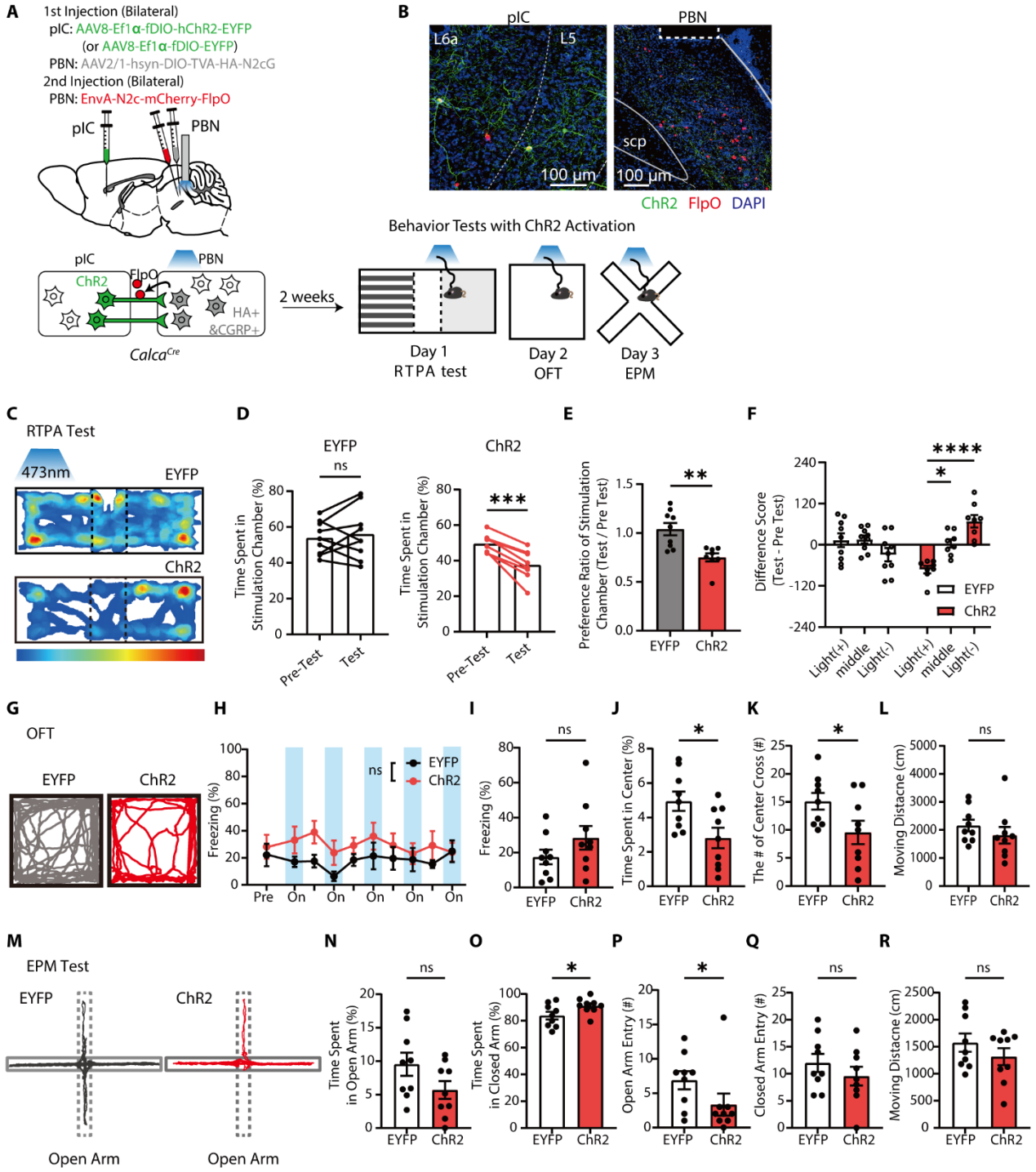

Fig. 8. Optogenetic stimulation of pIC$^{\rightarrow CGRP\text{-}PBN}$ projections in the PBN induces anxiogenic behaviors

(**A**) Schematic of viral injections and behavior tests. (**B**) Representative images of ChR2 (green) and/or retrogradely labeled FlpO (red) expression in the pIC (left) and PBN (right). The dotted rectangle marks the optic fiber location. (**C**) Representative heatmaps of time spent in RTPA test chambers during photostimulation. (**D-F**) ChR2 group avoided the photostimulation-paired chamber. (D) Time spent in the photostimulated chamber (Left, EYFP; N=9; Two-tailed paired t-test, t_8= 0.6490, P= 0.5345; Right, ChR2; N= 8, t_7= 6.837, P= 0.0002). (E) Preference ratio for the photostimulated chamber (Two-tailed Mann Whitney test, U= 6, P= 0.0025). (F) Difference score for each chamber (RM two-way ANOVA, Time × Group, $F_{2,30}$= 10.77, P= 0.0003). (**G**)

Representative movement trajectory during the OFT. (**H-L**) ChR2 photostimulation increased anxiety-like behaviors. (H) The photostimulation did not induce a freezing (EYFP, N= 9; ChR2, N= 9; RM two-way ANOVA, Time × Group, $F_{9,144}$= 0.8810, P= 0.5439). Averages of freezing levels (I) (Two-tailed unpaired t-test, t_{16}= 1.379, P= 0.1870), time spent in the center zone (J) (t_{16}= 2.627, P= 0.0183), number of center zone crossings (K) (t_{16}= 2.167, P= 0.0456), and moving distance (L) (t_{16}= 1.131, P= 0.2748). (**M**) Representative movement trajectory during EPM. (**N-R**) Time spent in open arms (N) (EYFP, N= 9; ChR2, N= 9; t_{16}= 1.406, P= 0.0894), time spent in closed arms (O) (t_{16}= 2.141, P= 0.0480), open arm entries (P) (U= 18.5, P= 0.0495), closed arm entries (Q) (t_{16}= 1.012, P=0.3267), and moving distance (R) (t_{16}= 1.129, P= 0.2757). Two-tailed Mann Whitney test in (P) and two-tailed unpaired t-test in (N, O, Q, R) were used. All data are mean ± s.e.m. *p < 0.05. **p < 0.01. ***p < 0.001. ****p < 0.0001. ns, not significant.

We next examined whether photostimulation of pIC$^{\rightarrow CGRP\text{-}PBN}$ projections in the PBN can serve as a US to drive threat conditioning. Using the same viral strategy, we selectively expressed ChR2 in pIC$^{\rightarrow CGRP\text{-}PBN}$ neurons (**Fig. 9, A, B, and fig. S4C**). During conditioning, photostimulation of these projections in the PBN was paired with the tone CS five times. In the tone retrieval test, only the ChR2 group exhibited increased freezing to the tone CS compared to the pre-CS period, while the EYFP control group did not (**Fig. 9C**). These findings demonstrate that pIC$^{\rightarrow CGRP\text{-}PBN}$ neurons transmit aversive affective information to the PBN and that this pathway is sufficient to drive threat conditioning, revealing a distinct circuit for threat learning.

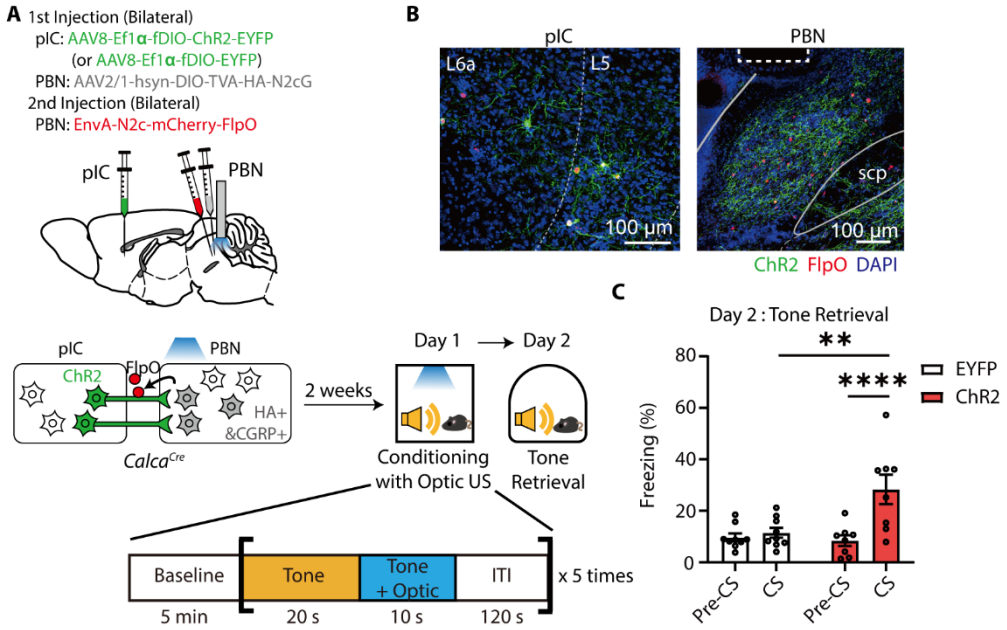

Fig. 9. Optogenetic stimulation of pIC$^{\rightarrow CGRP\text{-}PBN}$ projections in the PBN is sufficient to drive formation of fear memory

(**A**) Schematic of a threat conditioning paradigm with optogenetic stimulation of pIC$^{\rightarrow CGRP\text{-}PBN}$ projections in the PBN as s a US. During conditioning, mice were exposed to a 30-s tone, during which the last 10-s tone presentation was overlapped with optic stimulation. This CS-US pairing was repeated 5 times at a 120-s interval. (**B**) Representative images showing the neurons expressing ChR2 (green) and/or retrograde labeled FlpO (Red) in the pIC (left) and ChR2-expressing neurons projections (green) in the PBN (right). Neurons expressing FlpO were also detected in the PBN (right). The dotted rectangle indicates the location of the optic fiber. Scale bar, 100 μm. (**C**) ChR2-expressing mice exhibited increased freezing levels to the conditioned tone during the fear memory retrieval test (EYFP, N= 9; ChR2, N= 8; RM two-way ANOVA, Time × Group, $F_{1,15}$= 15.22, P= 0.0014). All data are mean ± s.e.m. **p < 0.01. ****p < 0.0001. ns, not significant.

Discussion

In this study, we established a visual threat conditioning model using looming stimuli as a US in mice. We demonstrated that CGRP^{PBN} neurons are essential for visual threat conditioning and play a broader role in fear learning across both nociceptive and non-nociceptive US. Additionally, we identified a distinct top-down pIC→CGRP^{PBN} circuit as a critical aversive US pathway required for visual threat conditioning. Both pIC$^{\rightarrow CGRP\text{-}PBN}$ and CGRP^{PBN} neurons exhibited threat-specific responses, and the pIC-PBN circuit was necessary for visual threat conditioning but dispensable for foot-shock conditioning. Moreover, activation of pIC$^{\rightarrow CGRP\text{-}PBN}$ projections in the PBN induced aversive affective states and was sufficient to drive fear memory formation. Given the monosynaptic connectivity between pIC and CGRP^{PBN} neurons, these findings suggest that the pIC→CGRP^{PBN} pathway functions as a primary US pathway for non-nociceptive danger signals.

CGRP^{PBN} neurons as a hub for threat assessment and fear learning

552 $CGRP^{PBN}$ neurons integrate external and internal signals for comprehensive threat
553 assessment, acting as a general danger-detection hub (*38*, *39*, *51*). They selectively
554 respond to threats like looming and foot shock but not to neutral stimuli (**Fig. 2, Fig. 6**),
555 highlighting their role in associative fear learning. After conditioning, their responses to
556 the tone CS increased (**Fig. 2M to O**), suggesting synaptic plasticity enables encoding of
557 learned danger. Both inactivation of $CGRP^{PBN}$ neurons during conditioning and retrieval
558 impaired conditioned freezing (**Fig. 3, G to L**), indicating their necessity for both fear
559 memory formation and recall, reinforcing their central role in visual threat conditioning.

560

561 **Distinct pIC-PBN pathway in encoding aversive states**

562 We found that the pIC-PBN pathway transmits aversive affective signals crucial
563 for visual threat conditioning. The $pIC^{\rightarrow CGRP\text{-}PBN}$ neurons selectively respond to both
564 visual and foot-shock threats, but not to neutral stimuli such as flickering (**Fig. 5**),
565 highlighting their role in processing aversive rather than neutral sensory input. Consistent
566 with this, human studies show that the insula is involved in both nociceptive and
567 psychological distress (*58*, *59*). These findings suggest that $pIC^{\rightarrow CGRP\text{-}PBN}$ neurons may
568 constitute a specific population that conveys affective pain signals from multimodal
569 sensory inputs to the PBN. Additionally, optogenetic activation of the $pIC^{\rightarrow CGRP\text{-}PBN}$
570 pathway induced an aversive state and drove fear memory formation in mice, reinforcing
571 its role in encoding aversive affect (**Fig. 8 and Fig. 9**).

572 Importantly, inhibition of the pIC-PBN pathway during the ITI impaired fear
573 memory formation (**Fig. 7J**), suggesting that sustained input from the pIC to PBN is
574 required for visual threat conditioning. This prolonged pIC activity may be maintained by
575 interoceptive inputs from physiological changes induced by threats. Indeed, activation of
576 SC parvalbumin-positive (PV+) neurons, which receive direct visual input from retinal
577 ganglion cells (RGCs) and selectively respond to looming threats, increases heart rate
578 (*71*), and $CGRP^{PBN}$ neurons contribute to tachycardia and anxiety-like behaviors (*72*).
579 Given the role of pIC in bottom-up cardiac interoceptive processing (*73*), physiological
580 signals may help maintain long-lasting pIC activity. Alternatively, local recurrent
581 connectivity, involving fast feedback inhibition and slow neuromodulatory transmission
582 (*74*, *75*), or bidirectional interactions with the PBN (*45*, *46*), could contribute to prolonged
583 activation.

584 In contrast, the pIC-PBN circuit was not essential for foot-shock conditioning (**Fig.
585 7H**). Additionally, silencing $pIC^{\rightarrow PBN}$ neurons disrupted $CGRP^{PBN}$ responses to looming
586 but not to foot shock (**Fig. 6**), suggesting that visual threats, which lack sensory pain,
587 primarily engage the pIC for aversive processing. Meanwhile, foot shocks, which involve
588 both affective and sensory pain, can recruit alternative pathways such as the spinal cord
589 and PAG to activate $CGRP^{PBN}$ neurons and support fear learning

590

591 **Dissociating innate defensive responses from learned fear**

592 A critical distinction in our study is the separation of innate defensive responses
593 and fear learning processes. $CGRP^{PBN}$ neurons were required for threat conditioning and
594 learned fear responses but not for immediate defensive behaviors to visual threats (**Fig. 3D
595 and fig. S2**). This aligns with studies showing that CGRP+ neurons in the thalamic
596 parvocellular subparafascicular nucleus ($CGRP^{SPFp}$), rather than $CGRP^{PBN}$ neurons,
597 mediate innate freezing to looming threats (*39*). Interestingly, $CGRP^{PBN}$ neurons are
598 required for innate freezing in response to other threat modalities, such as loud tones (*39*),

599 suggesting a modality-specific dissociation in defensive behaviors. Looming stimuli,
600 which mimic fast-approaching objects, likely elicit rapid, reflex-like reactions, whereas
601 fear learning requires a slower risk-assessment process mediated by the PBN.

602 The SC is a key structure in processing looming threats and coordinating
603 immediate defensive responses. SC PV+ neurons receive direct input from RGCs and
604 specifically respond to looming threats. Additionally, SC neurons transmit looming-
605 relevant inputs to multiple brain regions, including the PBGN, LPTN, PAG, and VTA,
606 which regulate immediate escape and freezing responses (*43*, *44*, *71*, *76*, *77*). Thus, an SC-
607 derived visual pathway, independent of $CGRP^{PBN}$ neurons, is likely responsible for
608 mediating looming-induced innate freezing.

609

610 **The presumed role of the SC-PBN pathway in visual threat processing**

611 Although we did not directly assess the function of the SC-PBN pathway, c-Fos
612 analysis revealed increased activity in $SC^{\rightarrow CGRP\text{-}PBN}$ neurons in response to looming
613 stimuli. Since SC neurons detect specific looming patterns in the visual field, the SC-PBN
614 pathway may rapidly transmit potential threat-related visual information to the PBN. It is
615 also possible that SC-PBN pathway is upstream of initial activation of $pIC^{\rightarrow CGRP\text{-}PBN}$
616 neurons, either directly or via intermediary structures. Given that $pIC^{\rightarrow CGRP\text{-}PBN}$ neurons
617 show increased activity during threat exposure (**Fig. 5**), the pIC likely receives visual
618 threat information rapidly. However, since the retina and SC lack known direct projections
619 to the pIC, visual signals may be relayed from the SC to the pIC via the PBN.
620 Alternatively, the pIC may receive threat-related signals from other intermediary
621 structures such as the thalamus and amygdala.

622 The functional role of SC-PBN in fear learning remains unknown. Future studies
623 should investigate the SC-PBN pathway's role in visual threat conditioning and clarify
624 where the neural circuits for innate freezing and threat conditioning diverge.

625

626 **Comparison to previous studies and unresolved questions**

627 A prior study reported a failure to achieve Pavlovian fear conditioning with
628 looming stimuli in rats (*78*), which differs from our findings in mice. This discrepancy
629 may stem from differences in experimental conditions, particularly the strong food drive
630 present in the prior study. $CGRP^{PBN}$ neurons integrate both hunger and danger signals, and
631 their suppression by hunger-related inputs (*79*, *80*) may have interfered with aversive
632 learning. Interestingly, the prior study found that combining looming with foot shock
633 successfully impaired food retrieval behavior, suggesting complementary roles for these
634 stimuli in recruiting fear-learning circuits. Future studies should explore how $CGRP^{PBN}$
635 neurons receive distinct inputs for different types of threats and how their activity is
636 modulated by physiological states.

637 Future research should examine whether the pIC-PBN circuit serves as a general
638 US circuit for non-nociceptive threats or is specific to visual stimuli. Additionally,
639 identifying the downstream targets of the pIC-PBN circuit responsible for mediating
640 aversive states and associative learning will be crucial. Since the fiber photometry
641 approach lacks single-cell resolution, it remains unclear whether individual $pIC^{\rightarrow PBN}$ and
642 $CGRP^{PBN}$ neurons respond to both visual and tactile inputs or if distinct subpopulations
643 exist for each modality. Given the role of $CGRP^{PBN}$ neurons in integrating affective

signals, investigating the human homologs of this circuit could provide valuable insights into therapeutic targets for anxiety and fear-related disorders.

Conclusion

Our findings reveal a top-down circuit mechanism by which non-nociceptive visual stimuli induce aversive behavioral states and drive fear memory formation. Identifying this distinct fear memory circuit broadens our understanding of how environmental threats shape fear memory and may inform treatments for threat-related neuropsychiatric disorders, including PTSD.

Materials and Methods

Mouse strains

Adult (8-24 weeks) C57BL/6J and heterozygous *Calca*^{Cre} (C57BL/6J) mice were used for experiments. Heterozygous *Calca*^{Cre} mice were generated by crossing homozygote *Calca*^{Cre} mice (JAX #033168) and C57BL/6J wild-type mice. Both male and female mice were used in balance, as we did not observe any noticeable differences in behaviors between male and female. Mice were group housed (3-5 mice per cage) under a 12 h light/dark cycle at a constant humidity (40-60%) and temperature (20-24°C). Food and water were available *ad libitum*. All procedures and protocols were approved by the KAIST Institutional Animal Care and Use Committee (KAIST IACUC, protocol # KA2020-16). All experiments were performed in accordance with the guideline of the KAIST Institutional Animal Care and Use Committee (KAIST IACUC).

Viruses

AAV1-hSyn-DIO-TeTox-P2A-nls-dTomato (5×10^{12} vg/ml), AAV1-hSyn-DIO-tdTomato (8×10^{11} vg/ml), AAV1-Ef1α-DIO-eNpHR3.0-EYFP (1×10^{12} vg/ml), AAV1-CaMKIIα-eNpHR3.0-EYFP (2.5×10^{12} vg/ml), AAV1-CaMKIIα-EGFP (2×10^{12} vg/ml), AAV8-hSyn-fDIO-mCehrry (8×10^{11} vg/ml), AAV8-Ef1α-fDIO-hChR2-EYFP (5×10^{13} vg/ml), AAV8-Ef1α-fDIO-EYFP (3×10^{13} vg/ml) were packaged.

AAV1-Ef1α-DIO EYFP (2×10^{13} vg/ml), AAV8-hSyn-fDIO-hM4Di-mCehrry (2.5×10^{13} vg/ml), AAVretro-Ef1α-FlpO (2.3×10^{13} vg/ml), AAV1-hsyn-DIO-GCaMP6m (1.9×10^{13} vg/ml), AAV8-Ef1α-fDIO-GCaMP6s (1.3×10^{13} vg/ml), AAV1-Ef1α-DIO-FlpO (2.1×10^{13} vg/ml) were purchased from Addgene. AAVdj-hsyn-fDIO-mGFP-2A-Synaptophysin-mRuby (1.9×10^{12} vg/ml) was purchased from Stanford gene vector and virus core (GVVC).

The helper and rabies viruses were obtained from the Viral Vector Core facility of the Kavli Institute for Systems Neuroscience, NTNU. The titers of each virus are as follows: AAV-hsyn-DIO-TVA-HA-N2cG (5×10^{11} vg/ml), EnvA pseudotyped SADB19 Rb GFP (1×10^{11} vg/ml), EnvA pseudotyped N2c Rb-mCherry-FlpO (4.4×10^{8} vg/ml). The helper virus was diluted to 5×10^{10} vg/ml in sterile DPBS (Gibco, ThermoFisher) before use for a specific Cre-dependent TVA expression as recommended by a previous paper (*81*).

Virus packaging

Adeno-associated virus (AAV) was packaged as previously described (*82*). The AAV DNA vector constructs used in this study were either obtained by subcloning of plasmids

690 or purchased from addgene. Briefly, we amplified and purified DNA plasmid by using
691 Maxiprep kit (QIAGEN). The prepared DNA vector was co-transfected with the viral
692 vector (pAd ΔF6 and AAV2/1 or AAV2/8) into HEK293T cells (ATCC, #CRL-3216) by
693 using calcium phosphate precipitation. Seventy-two hours after transfection, cells were
694 harvested, and virus was purified on iodixanol gradient by ultracentrifugation. Viral titers
695 were measured by qPCR (Rotor-Gene Q, QIAGEN).

696

697 **Stereotaxic surgeries**

698 Mice were anesthetized with intraperitoneal injection of pentobarbital (83 mg/kg of body
699 weight). Ophthalmic ointment (Liposic gel, BAUSCH and LOMB) was applied to the
700 eyes of the mice to prevent dehydration. Virus was injected with glass capillary filled with
701 water and 2µl of mineral oil (SIGMA, M5904-500ML) at the tip. The injection pipette was
702 placed at the injection site for additional 10 min post-surgery for diffusion of virus.

703 For manipulation of $CGRP^{PBN}$ neurons, $Calca^{Cre}$ mice receives bilateral injection of virus
704 (0.45µl per side) using the following coordinate: PBN (AP -5.0mm, ML ±1.4mm, DV -
705 3.55mm). For optogenetic inhibition of $CGRP^{PBN}$ neurons, the optic fibers (Doric lenses,
706 200µm core diameter, 0.37 NA for optogenetic manipulation) were implanted using the
707 following coordinate: PBN (AP -5.0mm, ML ±1.75mm, DV -3.1mm). For fiber
708 photometry of $CGRP^{PBN}$ neurons, the optic fiber (RWD, 400µm core diameter, 0.5 NA)
709 was implanted unilaterally on the right PBN. The mice underwent behavioral testing after
710 a 2-week recovery period.

711 For unilateral retrograde tracing, $Calca^{Cre}$ mice received unilateral injection of helper
712 virus (AAV-hsyn-DIO-TVA-HA-N2cG, 0.45µl) into the right hemisphere of PBN (AP -
713 5.0mm, ML +1.4mm, DV -3.55mm). Two weeks later, rabies virus (EnvA pseudotyped
714 SADB19 Rb GFP, 0.45µl) was injected into the same coordinate. Eight days later, mice
715 were sacrificed for histological analysis. For bilateral retrograde tracing and c-Fos
716 quantification, the injection surgeries were conducted on the bilateral PBN as above. Eight
717 days later, behavioral tests were performed, and mice were sacrificed for histological
718 analysis.

719 To inhibit terminals of pIC-PBN pathways, C57BL/6J mice received bilateral injection of
720 virus using the following coordinates: pIC (AP -0.4mm, ML ±4.2mm, DV -4.0mm, 0.4µl
721 per side). For optogenetic terminal inhibition, optic fiber (Doric Lenses, 200µm core
722 diameter, 0.37NA) was implanted right above the PBN (AP -5.0mm, ML ±1.75mm, DV -
723 3.1mm). Behavioral experiments were conducted 3 weeks after virus injection.

724 For fiber photometry of $CGRP^{PBN}$ neurons, AAV1-hsyn-DIO-GCaMP6m was unilaterally
725 injected into the right PBN (AP -5.0mm, ML +1.4mm, DV -3.55mm), and optic fiber
726 (RWD, 400µm core diameter, 0.5 NA) was implanted on the PBN (AP -5.0mm, ML
727 +1.75mm, DV -3.1mm). For fiber photometry of $CGRP^{PBN}$ neurons with hM4Di inhibition
728 of $pIC^{\rightarrow PBN}$ neurons, we bilaterally injected AAV8-hsyn-fDIO-hM4Di-mCehrry into the
729 pIC and AAVretro-Ef1α-FlpO into the PBN of $Calca^{Cre}$ mice. Ten days later, AAV1-
730 hsyn-DIO-GCaMP6m was unilaterally injected into the right PBN (AP -5.0mm, ML
731 +1.4mm, DV -3.55mm), and optic fiber (RWD, 400µm core diameter, 0.5 NA) was
732 implanted on the PBN (AP -5.0mm, ML +1.75mm, DV -3.1mm). After 2-week recovery
733 period, the fiber photometry experiments were conducted.

734 For fiber photometry of $pIC^{\rightarrow CGRP\text{-}PBN}$ neurons, helper virus (AAV-hS-DIO-TVA-HA-
735 N2cG, 0.45µl) was injected into the PBN (AP -5.0mm, ML +1.4mm, DV -3.55mm). Two
736 weeks later, the rabies virus (EnvA pseudotyped N2c Rb-mCherry-FlpO, 0.45µl) was

injected into the same site of PBN, and the AAV8-Ef1α-fDIO-GCaMP6s was injected into the ipsilateral pIC (AP -0.4mm, ML +4.2mm, DV -4.0mm, 0.4μl), respectively. Optic fiber (RWD, 400μm core diameter, 0.5 NA) was implanted on the pIC (AP -0.4mm, ML +4.2mm, DV -3.6mm). After a 2-week recovery period, the fiber photometry experiments were conducted.

For ChR2 activation of pIC-CGRP^{PBN} circuit, helper virus (AAV-hS-DIO-TVA-HA-N2cG, 0.45μl) was injected into the bilateral PBN (AP -5.0mm, ML ±1.4mm, DV -3.55mm, 0.45μl), and AAV8-Ef1α-fDIO-hChR2-EYFP was injected into the bilateral pIC (AP -0.4mm, ML ±4.2mm, DV -3.6mm, 0.4μl). Two weeks later, the rabies virus (EnvA pseudotyped N2c Rb-mCherry-FlpO, 0.45μl) was injected into the same site of bilateral PBN, and optic fibers (Doric Lenses, 200μm core diameter, 0.37NA) were implanted on the PBN (AP -5.0mm, ML ±1.75mm, DV -3.1mm). After a 2-week recovery period, the ChR2 activation experiments were conducted.

For axon tracing of PIC$^{\rightarrow PBN}$ neurons, we injected AAVretro-Ef1α-FlpO into the unilateral PBN, and AAVdj-hsyn-fDIO-mGFP-2A-Synaptophysin-mRuby into the ipsilateral side of pIC. After 3 weeks, the mice were sacrificed for histological analysis.

Behavioral procedures

Looming visual stimuli and behavioral apparatus

The looming visual stimuli were generated using custom software in the LabVIEW (National Instruments) environment and displayed on an overhead LCD monitor (38 cm × 22 cm, 60Hz refresh rate, Intehill). The monitor was positioned 30 cm above the mice and presented a white background. For the looming visual stimuli, a dark disc expanded from 5° (2.6 cm) to 35° (18.9 cm) of visual angle over 300 ms, remained on the screen for 500 ms, and was repeated five times (4 s) during conditioning and ten times (8 s) during the behavioral response test, respectively. For the flickering visual stimuli, a 35° (18.9 cm) dark disc appeared on the monitor for 0.8 s, disappeared for 0.8 s, and this sequence was repeated five times (8 s).

The behavioral arena was surrounded by white acrylic walls, with one of the four walls being transparent (35 cm long, 35 cm wide, 30 cm high). During the experiments, the mouse's behavior was recorded through the transparent wall using a video camera positioned diagonally over the arena. The video was captured at a frame rate of 30 FPS using LabVIEW software.

Innate behavioral responses to looming visual stimuli

All animals were handled for 3 days prior to behavioral tests. To assess innate defensive responses to looming visual stimuli, mice were moved to the behavioral arena from their home cages. After more than 2 min of baseline exploration period, mice were exposed to looming visual stimuli for 8 s (10 repetitions of an expanding dark disc). One minute after the exposure to the looming stimuli, animals were removed from the arena and returned to their home cages. To evaluate the habituation effect to the looming visual stimuli, the immediate response test was conducted for 5 consecutive days. In a single-day habituation test, mice were exposed to the visual stimuli ten times, with a 2-min interval between stimuli. The baseline freezing level was measured for 120 s during the pre-stimulus period before the onset of looming visual stimuli, and the looming-evoked freezing level was measured for 8 s during the visual stimuli presentation period.

783

784 ***Open-field test***

785 In the TetTox inhibition experiment, an open field test was performed prior to visual threat
786 conditioning to confirm that there were no differences in basal locomotion and anxiety
787 levels between groups. Mice were placed in an open field arena (45 cm long, 45 cm wide,
788 30 cm high) and allowed to freely explore for 15 min. Freezing levels, total distance
789 traveled, and time spent in the center area of the arena were measured.

790

791 ***Visual threat conditioning and fear memory retrieval test***

792 All animals were handled for 3 days prior to behavioral tests. The conditioning chamber
793 was a white acrylic box with one transparent wall, measuring 35 cm in length, 35 cm in
794 width, and 30 cm in height. The floor was covered with paper pads. After 5 min of
795 baseline exploration, mice were exposed to a 20-s auditory tone (CS, 2.7 kHz, 80 dB) that
796 was co-terminated with 4-s looming visual stimuli (US, a dark disc expanding five times).
797 After five CS-US pairings with a 2-min interval, mice were removed from the
798 conditioning chamber. In the unpaired conditioning protocol, the same auditory tone was
799 presented but with random intervals, ranging from 15 to 30 s after the looming visual
800 stimuli. The baseline freezing level was measured for 120 s during the pre-CS period
801 immediately before the tone onset. Freezing levels for the CS and CS+US periods were
802 measured during the first 16 s and last 4 s of CS-US pairing, respectively.

803 One day after conditioning, an auditory fear memory test was conducted. The mice were
804 placed in a test chamber with a shifted context: a semicircular arena, striped walls, and a
805 white acrylic floor (35 cm long, 35 cm wide, 30 cm high). After more than 2 min of
806 exploration, the conditioned tone was presented for 20 s. Freezing behavior was measured
807 during the pre-CS period (120 s) and the CS period (20 s).

808 Contextual fear memory test was conducted the following day. Mice were re-exposed to
809 the conditioning chamber for 5 min, and freezing behavior was measured during the first 2
810 min to assess contextual fear memory.

811

812 ***Foot-shock threat conditioning and fear memory retrieval test***

813 All mice underwent 3 days of handling prior to behavioral testing. For foot-shock
814 conditioning, mice explored a conditioning chamber equipped with a metal grid floor
815 (Med Associates, 25 cm long, 30 cm wide, 20 cm high) for 5 min. Subsequently, they
816 were exposed to a 20-s auditory tone (CS, 2.7 kHz, 80 dB) that was co-terminated with a
817 2-s foot-shock stimulus (US, 0.5 mA). The CS-US pairing was repeated 5 times with a 2-
818 min interval. The average of baseline movement was measured for 120 s during the pre-
819 CS period immediately before the onset of foot-shock. Movement for the CS and CS+US
820 periods was measured for the first 16 s and the last 4 s during CS-US pairing, respectively.

821 One day after foot-shock conditioning, an auditory fear memory test was conducted. Mice
822 were placed in a test chamber with a shifted context: a semicircular arena, striped walls,
823 and a white acrylic floor (Med Associates, 25 cm long, 30 cm wide, 20 cm high). After
824 more than 2 min of exploration, the conditioned tone was presented for 20 s. Freezing
825 behavior was measured during the pre-CS period (120 s) and the CS period (20 s).

826

827 ***Optogenetic inhibition behavior experiments***

All mice underwent three days of handling before behavioral testing. To habituate them to the optical manipulation procedure, they were tethered to fiber-optic patch cords for five minutes per day over three consecutive days.

For optogenetic eNpHR3.0 inhibition during conditioning, optical inhibition (561 nm, continuous; 3–5 mW at the fiber tip for soma inhibition, 10 mW for terminal inhibition) began two seconds before the first US exposure and continued until the end of the experiment.

For optogenetic inhibition during the tone retrieval test, optical inhibition was applied throughout the 20-second presentation of the tone-CS and terminated immediately afterward.

For optogenetic inhibition during the US exposure experiment, inhibition was initiated two seconds before US onset and terminated two seconds after US offset, lasting a total of eight seconds per trial.

For optogenetic inhibition during the ITI, inhibition started immediately after US exposure and ended just before the next US exposure, lasting two minutes per trial.

Optogenetic stimulation behavior experiments

All mice underwent 3 days of handling before behavioral testing. Additionally, mice were tethered to fiber-optic patch cords for 5 min per day over 3 consecutive days to habituate them to the optic manipulation procedure.

To assess the anxiogenic effects of stimulating the pIC-CGRP^{PBN} pathway, we conducted the RTPA test, open-field test, and elevated plus maze (EPM) test sequentially. In the RTPA test, the three-chamber arena was used (25 cm long, 75 cm wide, and 25 cm high; two side chambers with 30 cm wide each, and a middle chamber with 15 cm wide). One of the side chambers had a striped wall and metal grid floor, while the other had a checkered wall and punched metal floor. During the test, mice explored the arena for total 30 min. The first 10-min was used to determine a baseline chamber preference between the two side chambers. The chamber with more preference was selected for pairing with photostimulation. During the last 10 min, optical stimulation (473 nm, 20 Hz, 10 ms pulse, 10 mW at the fiber tip) was applied only when mice entered the selected side chamber. To assess the avoidance behavior induced by photostimulation, the time spent in each side chamber during the pre-test (the first 10 min) and test period (the last 10 min) was compared. The preference ratio was calculated by dividing the time spent in the photostimulation-paired chamber during the test by the time spent in the same chamber during the pre-test. The difference score was calculated by subtracting time spent in each chamber (left, middle, and right) during the pre-test from during the test. One mouse that spent more than 70% of the time in one of the two side chambers during the pre-test period was excluded from the analysis.

In the open-field test, to evaluate the effect of optical stimulation on immediate freezing and anxiogenic behaviors, mice were allowed to explore an open-field arena (45 cm x 45 cm x 30 cm). After 2-min exploration, the mice were exposed to a 30 s-photostimulation (473 nm, 20 Hz, 10 ms pulse, 10 mW at the fiber tip) session five times with a 60-s interval. Measures included freezing behavior, time spent in the center zone, the number of center crossings, and total distance traveled. The center zone was defined as a 20 cm square area in the center of the arena.

873 In the EPM test, the arena was a cross-shaped acrylic structure with 65 cm in length and 5
874 cm in width. Two closed arms were enclosed by 16 cm high white acrylic walls, while the
875 open arms have 0.5 cm high transparent acrylic walls. Mice were allowed to explore the
876 EPM arena freely for 10 min, during which they were exposed to photostimulation with a
877 2-s on and 2-s off cycle. To evaluate anxiety behavior, the time spent in the open and
878 closed arms, the number of entries into each arm, and the total distance traveled during the
879 10-min test were measured.

880 For optic conditioning, mice were allowed to explore a conditioning chamber equipped
881 with a metal grid floor (Med Associates, 25 cm long, 30 cm wide, 20 cm high) for 5 min.
882 Subsequently, they were exposed to a 30-s auditory tone (CS, 2.7 kHz, 80 dB) that was
883 co-terminated with a 10-s photostimulation (US, 473 nm, 20 Hz, 10 ms pulse, 10 mW at
884 the fiber tip). The CS-US pairing was repeated 5 times with a 2-min interval. One day
885 after conditioning, mice were tested for auditory fear memory. Mice were placed in a test
886 chamber with a shifted context: a semicircular arena, striped walls, and a white acrylic
887 (Med Associates, 25 cm long, 30 cm wide, 20 cm high). After more than 2 min of
888 exploration, the conditioned tone was presented for 30 s. Freezing behavior was measured
889 during the pre-CS period (120 s) and the CS period (30 s).

890

891 ***c-Fos imaging behavior experiments***

892 To assess c-Fos levels in the projection neurons upstream to $CGRP^{PBN}$ neurons in
893 response to looming visual stimuli, behavioral experiments were conducted 8 days after
894 rabies virus injection. Mice were allowed to freely explore the test arena for 5 min before
895 being exposed to visual stimuli (either looming visual stimuli for 8 s with 10 expansions
896 or flickering visual stimuli for 8 s with 5 flickers) twice at a 120-s interval. The mice were
897 then returned to their home cages and sacrificed 90 min after the first stimulus exposure.

898

899 **Fiber photometry**

900 For fiber photometry, a 400 μm diameter, 0.48 NA patch cord was used to collect
901 fluorescence emission. A real-time signal processor [Tucker-Davis Technologies (TDT),
902 RZ5P) controlled the 470 nm (Thor Labs, M470F3) and 405 nm (Doric, LEDC1-405_FC)
903 LEDs and simultaneously recorded GCaMP fluorescence emission. The 470 nm LED was
904 sinusoidally modulated at 331 Hz to excite GCaMP, while the 405 nm LED was
905 modulated at 531 Hz to monitor the isosbestic signal. The 470nm and 405nm light passed
906 through a bandpass filter in a mini cube (Doric, FMC5), and into the optic fiber connected
907 to the brain of mice. The emitted GCaMP6m signal was detected by a photoreceiver (New
908 Focus, Model 2151) and digitized at 1017.3 Hz by the RZ5P processor. Fluorescence
909 measurements (<6 Hz) were extracted from Synapse software (TDT), and further data
910 processing was performed in MATLAB. ΔF/F was calculated by applying a least-squares
911 linear fit to the 405 nm signal, aligning it with the 470 nm signal (fitted 405nm), and then
912 computing ΔF/F as (470 nm - fitted 405 nm)/fitted 405 nm.

913 Behavioral experiments were recorded at 30 FPS, with stimulus delivery and video
914 capture controlled by a custom LabView program. To synchronize photometry recording
915 with behavioral events (e.g., tone, visual stimuli, shock), digital signals generated by
916 LabView were recorded by the RZ5P processor.

917 To record calcium activity of $CGRP^{PBN}$ neurons in response to flickering and looming
918 visual stimuli, mice were placed in the looming test chamber and allowed to explore freely

919 for 5 minutes before stimulus presentation. First, they were exposed to flickering stimuli,
920 followed by looming stimuli after a 5-minute interval.

921 To examine calcium activity of $CGRP^{PBN}$ neurons while chemogenetically inhibiting
922 $pIC^{\rightarrow PBN}$ neurons, DREADD agonist 21 dihydrochloride (C21; Tocris, #6422; 0.2 mg/ml
923 working solution, 10 mg/ml stock) was administered via intraperitoneal injection at a dose
924 of 1 mg/kg. One hour after C21 injection, mice were placed in the looming test chamber,
925 where they explored for 5 minutes before being exposed to two looming stimuli (8 s) at a
926 120-second interval. After a 10-minute rest, mice were transferred to a foot-shock
927 chamber, where they explored for 5 minutes before receiving two foot-shocks (2 s, 0.5
928 mA) at a 120-second interval. To compare ΔF/F across animals during stimulus exposure,
929 ΔF/F was normalized to a Z-score, calculated as [(ΔF/F – Mean of $\Delta F/F_{baseline}$)/Std of
930 $\Delta F/F_{baseline}$], where the baseline mean and standard deviation were computed from –5 to 0
931 s before stimulus onset.

932 To record the calcium response of $pIC^{\rightarrow CGRP\text{-}PBN}$ neurons to visual or foot-shock stimuli,
933 mice were first placed in the looming test chamber, where they explored freely for five
934 minutes before being exposed to looming visual stimuli (or flickering stimuli). The
935 looming (or flickering) stimuli presented twice at a 120-s interval. After a 10-minute rest
936 period, mice were transferred to the foot-shock chamber, where they explored freely for
937 five minutes before receiving two foot-shocks (2 s, 0.5 mA) at a 120-s interval. As
938 $pIC^{\rightarrow CGRP\text{-}PBN}$ neurons exhibited sustained calcium activity in response to both looming
939 and shock stimuli, only the first 60 seconds of recording data from stimulus onset were
940 included in the analysis. To minimize the effect of natural fluctuations in pIC neuronal
941 activity, the baseline for Z-scoring was computed from the 60-second period preceding
942 stimulus onset (–60 to 0 s). To determine the peak and the time to half of the peak in
943 calcium activity, Z-scored calcium activity was filtered using a 1 Hz low-pass filter. The
944 maximum peak was identified within the 0–100 s time window following stimulus onset.
945 After determining the peak time, the time point at which calcium activity declined to half
946 of the peak value was identified. Since $pIC^{\rightarrow CGRP\text{-}PBN}$ neurons exhibited persistent but
947 distinct response dynamics to looming and shock stimuli, we analyzed their responses
948 based on the half-peak time window: 0–60 s for looming and 0–20 s for shock

949

950 **Analysis of behaviors**

951 Freezing was defined as a state in which the mouse remained completely immobile except
952 for respiratory movements. Running was defined as when the centroid of the mouse body
953 moved at a velocity of 40 cm/s or greater. All other behaviors were classified as no
954 response. The centroid of the subjects was analyzed to determine position, calculate
955 velocity, and track movement trajectories. Centroid was detected by using custom
956 MATLAB scripts. Brightness thresholds were manually set to differentiate the pixels
957 corresponding to the mouse. Perspective distortion from the camera lens was corrected
958 using the *tform* function in MATLAB. Velocity was calculated from the centroid data and
959 smoothed using a mean filter.

960

961 **Histology**

962 For histological verification of virus expression and optic fiber placement, brain sections
963 were prepared from the sacrificed mice after the end of behavioral experiments. Mice
964 were anesthetized with 2.5% avertin by intraperitoneal injection, and they were perfused
965 transcardially with phosphate-buffered saline (PBS) and then fixed with ice cold 4%

966 paraformaldehyde (PFA). After perfusion, brain samples were stored in 4% PFA overnight
967 for post-fixation and sliced in a 40μm thickness afterward by using a vibratome (VT-
968 1200S, Leica Microsystems).

969 For a retrograde tracing and c-Fos staining, mice underwent behavioral experiments 8
970 days after the rabies virus injection and were sacrificed 90 min after exposure to visual
971 stimuli. Mice were anesthetized with pentobarbital (83 mg/kg of body weight) by
972 intraperitoneal injection, perfused transcardially with phosphate-buffered saline (PBS),
973 and then fixed with ice cold 4% paraformaldehyde (PFA). After perfusion, brain samples
974 were stored in 4% PFA overnight for post-fixation. Fixed brain samples were dehydrated
975 in a series of 10%, 20%, and 30% filtered sucrose solutions (#S0389, Sigma-Aldrich) until
976 they sank to the bottom of vials. Dehydrated brain samples were attached on a specimen
977 disc with OCT compounds (#4583, Scigen) at -20 °C. Brains were coronally sliced in a
978 40μm thickness by using a Cryostat (Leica CM1850, Leica Biosystems).

979 Brain sections were mounted on a gelatin-coated slide glass with a Vectashield antifade
980 mounting media (h-2000, Vector Laboratories). Images were taken for histological
981 verification by using a confocal microscope (LSM880, Carl ZEISS) or slide scanner
982 (ZEISS Axio Scan.Z1, Carl ZEISS). By reference to the Mouse Brain Atlas, the mice who
983 showed off-target viral expression in surrounding areas or displacement of ferrules were
984 excluded.

985

986 **Immunohistochemistry**

987 For immunostaining, brain sections were washed three times with PBS and incubated in
988 blocking solution (2% goat serum, 0.1% BSA, and 0.2% Triton X-100 in PBS) for 1 hour
989 on an orbital shaker (126 rpm). Brain sections were incubated in a primary antibody
990 solution on the orbital shaker (126 rpm) overnight at room temperature (RT). After brain
991 sections were washed four times with PBS, sections were then incubated in a secondary
992 antibody solution on the shaker (126 rpm) for 2 hours. Subsequently, the brain sections
993 underwent four additional washes with PBS. Immunostained brain sections were
994 transferred to gelatin-coated slides using a brush. Sections were stained with DAPI
995 (0.5μg/ml in PBS; #D9542, Sigma-Aldrich) for 20min at RT. The slides were rapidly
996 immersed in a distilled water and allowed to air-dry completely in a light-protected
997 environment. Coverslip was mounted with a Vectashield antifade mounting media (h-
998 2000, Vector Laboratories).

999 The dTomato fluorescence signals in neurons injected with AAV-TetTox-P2A-nls-
1000 dTomato virus were amplified with mouse anti-DsRed primary antibody (1:500; #SC-
1001 390909, Santacruz) and Alexa Fluor 594-conjugated goat anti-mouse secondary antibody
1002 (1:2000; #A-11005, Molecular Probes). The EYFP fluorescence signals in neurons
1003 injected with AAV-CaMKIIα-eNpHR3.0-EYFP virus were amplified with rabbit anti-GFP
1004 primary antibody (1:5000; #ab290, abcam) and Alexa Fluor 488-conjugated goat anti-
1005 rabbit secondary antibody (1:2000; #A-11008, Molecular Probes). The antibodies used for
1006 HA staining were rabbit anti-HA (1:1000; #3724, Cell signaling) and Alexa Fluor 647-
1007 conjugated goat anti-rabbit (1:2000; #A-21244, Molecular Probes). The antibodies used
1008 for c-Fos staining were rabbit anti-cFos (rabbit anti-cFos; 1:2000; #226008, Synaptic
1009 systems) and Alexa Fluor 594-conjugated goat anti-rabbit (Alexa Fluor 594-conjugated
1010 goat anti-rabbit; 1:2000; #A-11037, Molecular Probes). In axon tracing experiment, mGFP
1011 and synaptophysin-mRuby were amplified with rabbit anti-GFP primary antibody (1:5000;
1012 #ab290, abcam), mouse anti-RFP primary antibody (1:2000; # 200-301-379; Rockland),
1013 Alexa Fluor 488-conjugated goat anti-rabbit secondary antibody (1:2000; #A-11008,

Molecular Probes), and Alexa Fluor 594-conjugated goat anti-mouse (1:2000; #A-11005, Molecular Probes).

For anterograde tracing of the pIC$^{\rightarrow PBN}$ neurons, Sudan black B (SBB) staining was performed. After DAPI staining, the samples were stained with 0.1% SBB for 20 minutes at room temperature. The sections were briefly rinsed with 70% ethanol for 30 seconds, followed by a 5-minute rinse in PBS. The 0.3% SBB stock solution (in 70% ethanol) was stirred overnight in the dark and filtered using a 0.22µm filter. The 0.1% SBB working solution was freshly prepared before use.

Cell counting analysis

To map the location of retrogradely labeled GFP+ cells throughout the whole brain, coronal brain tissues were collected along AP axis (from anterior part AP +1.8 mm to posterior part AP: -5.5 mm) in a 120-µm distance. For the brain-wide tracing, images of all brain sections were captured using a Slide scanner (ZEISS Axio Scan.Z1, Carl ZEISS). The number of DAPI+ and GFP+ cells in the brain sections were then counted by using the AMaSiNe automatic cell counting software (*83*) by registering brain images to the Allen Brain Atlas Common Coordinate Framework (CCFv3) (*84*).

To assess the overlap between c-Fos+ and GFP+ cells, we conducted c-Fos immunostaining, and optical sections (2 µm per section) were obtained using confocal microscopy with Z-stack analysis. DAPI+, GFP+, and c-Fos+ cells were detected using the AMaSiNe cell counting algorithm (*83*). Regions of interest (ROI) were then defined in each target area, and the overlap between c-Fos+ and GFP+ cells was manually counted in a blinded manner. The AP ranges for c-Fos quantification in each target brain area are: pIC (AP -0.2 to -0.6 mm), CeA (AP -1.2 to -1.6 mm), PAG (AP -3.5 to -3.9 mm), SC (AP -3.5 to -3.9 mm).

To compare CGRP^{PBN}-projecting neurons in the aIC and pIC, we counted GFP+ cells in the aIC (AP: +1.0 to 0 mm) and pIC (AP: 0 to -1.0 mm).

Statistical analysis

GraphPad Prism 10.0.2 was used for graph generation and statistical analyses. The Shapiro-Wilk test was used to assess data normality. For datasets with a small sample size ($N < 7$), the Kolmogorov-Smirnov test was conducted, and data distribution was additionally evaluated using QQ-plots. Paired or unpaired Student's t-tests were performed to compare normally distributed datasets of experimental and control groups depending on experimental design. Wilcoxon matched-pairs signed rank test or Mann Whitney test were performed to compare non-normally distributed datasets of experimental and control groups. One-way ANOVA and repeated-measures two-way ANOVA, followed by Sidak's post-hoc test, were used to analyze behavioral tasks depending on the experimental design. Differences were considered statistically significant if the p-value was below 0.05. Error bars represent the s.e.m.

References

1. T. Beckers, D. Hermans, I. Lange, L. Luyten, S. Scheveneels, B. Vervliet, Understanding clinical fear and anxiety through the lens of human fear conditioning. *Nat. Rev. Psychol.* **2**, 233-245 (2023).

1060 2. J. E. LeDoux, Emotion, memory and the brain. *SCI AM* **270**, 50-57 (1994).

1061 3. M. S. Fanselow, What is conditioned fear?. *TINS* **7**, 460-462 (1984).

1062 4. J. E. LeDoux, Emotion circuits in the brain. Annu. Rev. Neurosci. **23**, 155-184 (2000).

1063 5. J. F. Medina, J. Christopher Repa, M. D. Mauk, J. E. LeDoux, Parallels between cerebellum-and
1064 amygdala-dependent conditioning. *Nat. Rev. Neurosci.* **3**, 122-131 (2002).

1065 6. J. P. Johansen, C. K. Cain, L. E. Ostroff, J. E. LeDoux, Molecular mechanisms of fear learning
1066 and memory. *Cell* **147**, 509-524 (2011).

1067 7. C. T. Gross, N. S. Canteras, The many paths to fear. *Nat. Rev. Neurosci.* **13**, 651-658 (2012).

1068 8. P. Tovote, J. P. Fadok, A. Lüthi, Neuronal circuits for fear and anxiety. *Nat. Rev. Neurosci.* **16**,
1069 317-331 (2015).

1070 9. L. K. Takahashi, M. M. Chan, M. L. Pilar, Predator odor fear conditioning: current perspectives
1071 and new directions. *Neurosci Biobehav Rev* **32**, 1218-1227 (2008).

1072 10. D. C. Blanchard, G. Griebel, R. J. Blanchard, Conditioning and residual emotionality effects of
1073 predator stimuli: some reflections on stress and emotion. *Prog Neuropsychopharmacol Biol Psychiatry*
1074 **27**, 1177-1185 (2003).

1075 11. M. Yilmaz, M. Meister, Rapid innate defensive responses of mice to looming visual stimuli. *Curr.*
1076 *Biol.* **23**, 2011-2015 (2013).

1077 12. L. K. Takahashi, D. T. Hubbard, I. Lee, Y. Dar, S. M. Sipes, Predator odor-induced conditioned
1078 fear involves the basolateral and medial amygdala. *Behav. Neurosci.* **121**, 100 (2007).

1079 13. N. S. Pentkowski, D. C. Blanchard, C. Lever, Y. Litvin, R. J. Blanchard, Effects of lesions to the
1080 dorsal and ventral hippocampus on defensive behaviors in rats. *EJN* **23**, 2185-2196 (2006).

1081 14. D. C. Blanchard, N. S. Canteras, C. M. Markham, N. S. Pentkowski, R. J. Blanchard, Lesions of
1082 structures showing FOS expression to cat presentation: effects on responsivity to a Cat, Cat odor, and
1083 nonpredator threat. *Neurosci Biobehav Rev* **29**, 1243-1253 (2005).

1084 15. M. Rodríguez, F. Ceric, P. Murgas, B. Harland, F. Torrealba, M. Contreras, Interoceptive insular
1085 cortex mediates both innate fear and contextual threat conditioning to predator odor. *Front. behav.*
1086 *neurosci.* **13**, 283 (2020).

1087 16. K. J. Wallace, J. B. Rosen, Predator odor as an unconditioned fear stimulus in rats: elicitation of
1088 freezing by trimethylthiazoline, a component of fox feces. *Behav. Neurosci.* **114**, 912 (2000).

1089 17. R. J. Blanchard, M. Yang, C. I. Li, A. Gervacio, D. C. Blanchard, Cue and context conditioning of
1090 defensive behaviors to cat odor stimuli. *Neurosci Biobehav Rev* **25**, 587-595 (2001).

1091 18. L. K. Takahashi, Olfactory systems and neural circuits that modulate predator odor fear. *Front.*
1092 *behav. neurosci.* **8**, 72 (2014).

1093 19. A. Cruz, M. Heinemans, C. Marquez, M. A. Moita, Freezing displayed by others is a learned cue
1094 of danger resulting from co-experiencing own freezing and shock. *Curr. Biol.* **30**, 1128-1135 (2020).

1095 20. D. C. Blanchard, C. Markham, M. Yang, D. Hubbard, E. Madarang, R. J. Blanchard, Failure to
1096 produce conditioning with low-dose trimethylthiazoline or cat feces as unconditioned stimuli. *Behav.*
1097 *Neurosci.* **117**, 360 (2003).

1098 21. G. De Franceschi, T. Vivattanasarn, A. B. Saleem, S. G. Solomon, Vision guides selection of
1099 freeze or flight defense strategies in mice. *Curr. Biol.* **26**, 2150-2154 (2016).

1100 22. G. Baranauskas, N. Svirskiene, G. Svirskis, 20 Hz membrane potential oscillations are driven by
1101 synaptic inputs in collision-detecting neurons in the frog optic tectum. *Neurosci. Lett.* **528**, 196-200
1102 (2012).

1103 23. T. W. Dunn, C. Gebhardt, E. A. Naumann, C. Riegler, M. B. Ahrens, F. Engert, F. Del Bene,
1104 Neural circuits underlying visually evoked escapes in larval zebrafish. *Neuron* **89**, 613-628 (2016).

1105 24. K. Bhattacharyya, D. L. McLean, M. A. MacIver, Visual threat assessment and reticulospinal
1106 encoding of calibrated responses in larval zebrafish. *Curr. Biol.* **27**, 2751-2762 (2017).

1107 25. W. Schiff, J. A. Caviness, J. J. Gibson, Persistent fear responses in rhesus monkeys to the optical
1108 stimulus of "looming". *Science* **136**, 982-983 (1962).

1109 26. J. Náñez Sr, Perception of impending collision in 3-to 6-week-old human infants. *Infant Behav.*
1110 *Dev.* **11**, 447-463 (1988).

1111 27. W. Schiff, Perception of impending collision: A study of visually directed avoidant
1112 behavior. *Psychol. Monogr.* **79**, 1 (1965).

1113 28. S. Maren, Neurobiology of Pavlovian fear conditioning. *Annu. Rev. Neurosci.***24**, 897-931 (2001).

1114 29. B. A. Pellman, J. J. Kim, What can ethobehavioral studies tell us about the brain's fear
1115 system? *TINS* **39**, 420-431 (2016).

1116 30. J. E. LeDoux, Coming to terms with fear. *Proc. Natl. Acad. Sci. U.S.A.* **111**, 2871-2878 (2014).

1117 31. H. C. Pape, D. Pare, Plastic synaptic networks of the amygdala for the acquisition, expression, and
1118 extinction of conditioned fear. *Physiol. Rev.* **90**, 419-463 (2010).

1119 32. R. P. Vertes, S. B. Linley, W. B. Hoover, Limbic circuitry of the midline thalamus. *Neurosci*
1120 *Biobehav Rev* **54**, 89-107 (2015).

1121 33. L. G. Reijmers, B. L. Perkins, N. Matsuo, M. Mayford, Localization of a stable neural correlate of
1122 associative memory. *Science* **317**, 1230-1233 (2007).

1123 34. P. W. Frankland, B. Bontempi, L. E. Talton, L. Kaczmarek, A. J. Silva, The involvement of the
1124 anterior cingulate cortex in remote contextual fear memory. *Science* **304**, 881-883 (2004).

1125 35. J. A. Boatman, J. J. Kim, A thalamo-cortico-amygdala pathway mediates auditory fear
1126 conditioning in the intact brain. *EJN* **24**, 894-900 (2006).

1127 36. J. P. Johansen, H. L. Fields, Glutamatergic activation of anterior cingulate cortex produces an
1128 aversive teaching signal. *Nat. Neurosci.* **7**, 398-403 (2004).

1129 37. S. Han, M. T. Soleiman, M. E. Soden, L. S., Zweifel, R. D. Palmiter, Elucidating an affective pain
1130 circuit that creates a threat memory. *Cell* **162**, 363-374 (2015).

1131 38. C. A. Campos, A. J. Bowen, C. W. Roman, R. D. Palmiter, Encoding of danger by parabrachial
1132 CGRP neurons. *Nature* **555**, 617-622 (2018).

1133 39. S. J. Kang, S. Liu, M. Ye, D. I. Kim, G. M. Pao, B. A. Copits, B. Z. Roberts, K. F. Lee, M. R.
1134 Bruchas, S. Han, A central alarm system that gates multi-sensory innate threat cues to the
1135 amygdala. *Cell Rep.* **40**, (2022).

1136 40. K. E. Krout, A. S. Jansen, A. D. Loewy, Periaqueductal gray matter projection to the parabrachial
1137 nucleus in rat. *J. Comp. Neurol.* **401**, 437-454 (1998).

1138 41. A. J. Todd, Neuronal circuitry for pain processing in the dorsal horn. *Nat. Rev. Neurosci.* **11**, 823-
1139 836 (2010).

1140 42. S. P. Hunt, P. W. Mantyh, The molecular dynamics of pain control. *Nat. Rev. Neurosci.* **2**, 83-91
1141 (2001).

1142 43. C. Shang, Z. Chen, A. Liu, Y. Li, J. Zhang, B. Qu, F. Yan, Y. Zhang, W. Liu, Z. Liu, X. Guo, D.
1143 Li, Y. Wang, P. Cao, Divergent midbrain circuits orchestrate escape and freezing responses to looming
1144 stimuli in mice. *Nat. Commun.* **9**, 1232 (2018).

1145 44. P. Wei, N. Liu, Z. Zhang, X. Liu, Y. Tang, X. He, B. Wu, Z. Zhou, Y. Liu, J. Li, Y. Zhang, X.
1146 Zhou, L. Xu, L. Chen, G. Bi, X. Hu, F. Xu, L. Wang, Processing of visually evoked innate fear by a
1147 non-canonical thalamic pathway. *Nat. Commun.* **6**, 6756 (2015).

1148 45. T. L. Krukoff, K. H. Harris, J. H. Jhamandas, Efferent projections from the parabrachial nucleus
1149 demonstrated with the anterograde tracer Phaseolus vulgaris leucoagglutinin. *BRB* **30**, 163-172 (1993).

1150 46. K. Tokita, T. Inoue, J. D. Boughter Jr., Afferent connections of the parabrachial nucleus in
1151 C57BL/6J mice. *Neuroscience* **161**, 475-488 (2009).

1152 47. P. Rainville, B. Carrier, R. K. Hofbauer, M. C. Bushnell, G. H. Duncan, Dissociation of sensory
1153 and affective dimensions of pain using hypnotic modulation. *Pain* **82**, 159-171 (1999).

1154 48. T. Singer, B. Seymour, J. O'doherty, H. Kaube, R. J. Dolan, C. D. Frith, Empathy for pain involves
1155 the affective but not sensory components of pain. *Science* **303**, 1157-1162 (2004).

1156 49. D. D. Price, Psychological and neural mechanisms of the affective dimension of pain. *Science* **288**,
1157 1769-1772 (2000).

1158 50. A. C. de. C. Williams, K. D. Craig, Updating the definition of pain. *Pain* **157**, 2420-2423 (2016).

1159 51. R. D. Palmiter, The parabrachial nucleus: CGRP neurons function as a general alarm. *TINS* **41**,
1160 280-293 (2018).

1161 52. M. E. Carter, M. E. Soden, L. S. Zweifel, R. D. Palmiter, Genetic identification of a neural circuit
1162 that suppresses appetite. *Nature* **503**, 111-114 (2013).

1163 53. J. C. Kim, M. N. Cook, M. R. Carey, C. Shen, W. G. Regehr, S. M. Dymecki, Linking genetically
1164 defined neurons to behavior through a broadly applicable silencing allele. *Neuron* **63**, 305-315 (2009).

1165 54. D. C. Castro, K. C. Berridge, Opioid and orexin hedonic hotspots in rat orbitofrontal cortex and
1166 insula. *PNAS* **114**, E9125–E9134 (2017).

1167 55. Y. Peng, S. Gillis-Smith, H. Jin, D. Tränkner, N. J. P. Ryba, C. S. Zuker, Sweet and bitter taste in
1168 the brain of awake behaving animals. *Nature* **527**, 512–515 (2015).

1169 56. D. A. Gehrlach, N. Dolensek, A. S. Klein, R. R. Chowdhury, A. Matthys, M. Junghänel, T. N.
1170 Gaitanos, A. Podgornik, T. D. Black, N. R. Vaka, K.-K. Conzelmann, N. Gogolla, Aversive state
1171 processing in the posterior insular cortex. *Nat. Neurosci.* **22**, 1424-1437 (2019).

1172 57. M. P. Paulus, M. B. Stein, An insular view of anxiety. *Biol Psychiatry* **60**, 383-387 (2006).

1173 58. H. Gündel, M. F. O'Connor, L. Littrell, C. Fort, R. D. Lane, Functional neuroanatomy of grief: an
1174 FMRI study. *Am J Psychiatry* **160**, 1946-1953 (2003).

1175 59. N. I. Eisenberger, M. D. Lieberman, K. D. Williams, Does rejection hurt? An fMRI study of social
1176 exclusion. *Science* **302**, 290-292 (2003).

1177 60. N. Grahek, *Feeling pain and being in pain. mit Press* (2011)

1178 61. A. S. Klein, N. Dolensek, C. Weiand, N. Gogolla, Fear balance is maintained by bodily feedback
1179 to the insular cortex in mice. *Science* **374**, 1010-1015 (2021).

1180 62. J. B. Nitschke, I. Sarinopoulos, K. L. Mackiewicz, H. S. Schaefer, R. J. Davidson, Functional
1181 neuroanatomy of aversion and its anticipation. *Neuroimage* **29**, 106-116 (2006).

1182 63. T. Klucken, S. Kagerer, J. Schweckendiek, K. Tabbert, D. Vaitl, R. Stark, Neural, electrodermal
1183 and behavioral response patterns in contingency aware and unaware subjects during a picture–picture
1184 conditioning paradigm. *Neurosci.* **158**, 721-731 (2009).

1185 64. Y. Livneh, A. U. Sugden, J. C. Madara, R. A. Essner, V. I. Flores, L. A. Sugden, J. M. Resch, B.
1186 B. Lowell, M. L. Andermann, Estimation of Current and Future Physiological States in Insular Cortex.
1187 *Neuron* **105**, 1094-1111.e10 (2020).

1188 65. Y. Livneh, M. L. Andermann, Cellular activity in insular cortex across seconds to hours:
1189 Sensations and predictions of bodily states. *Neuron* **109**, 3576-3593 (2021).

1190 66. X. Chen, H. Choo, X. P. Huang, X. Yang, O. Stone, B. L. Roth, J. Jin, The first structure–activity
1191 relationship studies for designer receptors exclusively activated by designer drugs. *ACS Chem.*
1192 *Neurosci.* **6**, 476-484 (2015).

1193 67. H. Li, M. A. Penzo, H. Taniguchi, C. D. Kopec, Z. J. Huang, B. Li, Experience-dependent
1194 modification of a central amygdala fear circuit. *Nat Neurosci* **16**, 332–339 (2013).

1195 68. A. Adhikari, T. N. Lerner, J. Finkelstein, S. Pak, J. H. Jennings, T. J. Davidson, E. Ferenczi, L. A.
1196 Gunaydin, J. J. Mirzabekov, L. Ye, S. Y. Kim, A. Lei, K. Deisseroth, Basomedial amygdala mediates
1197 top-down control of anxiety and fear. *Nature* **527**, 179–185 (2015).

1198 69. T. Nagashima, S. Tohyama, K. Mikami, M. Nagase, M. Morishima, A. Kasai, H. Hashimoto, A.
1199 M. Watabe, Parabrachial-to-parasubthalamic nucleus pathway mediates fear-induced suppression of
1200 feeding in male mice. *Nat Commun* **13,** 7913 (2022).

1201 70. J. P. Johansen, J. W. Tarpley, J. E. Ledoux, H. T. Blair, Neural substrates for expectation-
1202 modulated fear learning in the amygdala and periaqueductal gray. *Nat Neurosci* **13**, 979–986 (2010).

1203 71. C. Shang, Z. Liu, Z. Chen, Y. Shi, Q. Wang, S. Liu, D. Li, P. Cao, A parvalbumin-positive
1204 excitatory visual pathway to trigger fear responses in mice. *Science* **348**, 1472-1477 (2015).

1205 72. A. J. Bowen, J. Y. Chen, Y. W. Huang, N. A. Baertsch, S. Park, R. D. Palmiter, Dissociable
1206 control of unconditioned responses and associative fear learning by parabrachial CGRP neurons. *Elife* **9**,
1207 e59799 (2020).

1208 73. B. Hsueh, R. Chen, Y. Jo, D. Tang, M. Raffiee, Y. S. Kim, M. Inoue, S. Randles, C.
1209 Ramakrishnan, S. Patel, D. K. Kim, T. X. Liu, S. H. Kim, L. Tan, L. Mortazavi, A. Cordero, J. Shi, M.
1210 Zhao, T. T. Ho, A. Crow, A.-C. W. Yoo, C. Raja, K. Evans, D. Bernstein, M. Zeineh, M. Goubran, K.
1211 Deisseroth, Cardiogenic control of affective behavioural state. *Nature* **615**, 292-299 (2023).

1212 74. A. Kennedy, P. S. Kunwar, L. yun Li, S. Stagkourakis, D. A. Wagenaar, D. J. Anderson, Stimulus-
1213 specific hypothalamic encoding of a persistent defensive state. *Nature* **586**, 730–734 (2020).

1214 75. Y. N. Jan, L. Y. Jan, S. W. Kuffler, A peptide as a possible transmitter in sympathetic ganglia of
1215 the frog. *PNAS* **76**, 1501-1505 (1979).

1216 76. D. A. Evans, A. V. Stempel, R. Vale, S. Ruehle, Y. Lefler, T. Branco, A synaptic threshold
1217 mechanism for computing escape decisions. *Nature* **558**, 590-594 (2018).

1218 77. Z. Zhou, X. Liu, S. Chen, Z. Zhang, Y. Liu, Q. Montardy, Y. Tang, P. Wei, N. Liu, L. Li, R. Song,
1219 J. Lai, X. He, C. Chen, G. Bi, G. Feng, F. Xu, L. Wang, VTA GABAergic neural circuit mediates
1220 visually evoked innate defensive responses. *Neuron* **103**, 473-488 (2019).

1221 78. P. R. Zambetti, B. P. Schuessler, B. E. Lecamp, A. Shin, E. J. Kim, J. J. Kim, Ecological analysis
1222 of Pavlovian fear conditioning in rats. *Commun Biol* **5**, 830 (2022).

1223 79. R. A. Essner, A. G. Smith, A. A. Jamnik, A. R. Ryba, Z. D. Trutner, M. E. Carter, AgRP neurons
1224 can increase food intake during conditions of appetite suppression and inhibit anorexigenic parabrachial
1225 neurons. *Journal of Neuroscience* **37**, 8678–8687 (2017).

1226 80. A. L. Alhadeff, Z. Su, E. Hernandez, M. L. Klima, S. Z. Phillips, R. A. Holland, C. Guo, A. W.
1227 Hantman, B. C. De Jonghe, J. N. Betley, A Neural Circuit for the Suppression of Pain by a Competing
1228 Need State. *Cell* **173**, 140-152.e15 (2018).

1229 81. T. J. Roelofs, S. Menting-Henry, L. M. Gol, A. M. Speel, V. H. Wielenga, K. M. Garner, M. C. M.
1230 Luijendijk, A. A. Hennrich, K. K. Conzelmann, R. A. Adan, Optimization of whole-brain rabies virus
1231 tracing technology for small cell populations. *Sci. Rep.* **11**, 10400 (2021).

1232 82. J. T. Kwon, R. Nakajima, H. S. Kim, Y. Jeong, G. J. Augustine, J. H. Han, Optogenetic activation
1233 of presynaptic inputs in lateral amygdala forms associative fear memory. *Learn. Mem.* **21**, 627-633
1234 (2014).

1235 83. J. H. Song, W. Choi, Y. H. Song, J. H. Kim, D. Jeong, S. H. Lee, S. B. Paik, Precise mapping of
1236 single neurons by calibrated 3D reconstruction of brain slices reveals topographic projection in mouse
1237 visual cortex. *Cell Rep.* **31**, (2020).

1238 84. Q. Wang, S. L. Ding, Y. Li, J. Royall, D. Feng, P. Lesnar, N. Graddis, M. Naeemi, B. Facer, A.
1239 Ho, T. Dolbeare, B. Blanchard, N. Dee, W. Wakeman, K. E. Hirokawa, A. Szafer, S. M. Sunkin, S. W.
1240 Oh, A. Bernard, J. W. Phillips, M. Hawrylycz, C. Koch, H. Zeng, J. A. Harris, L. Ng, The Allen mouse
1241 brain common coordinate framework: a 3D reference atlas. *Cell* **181**, 936-953 (2020).

Acknowledgments

We thank all members of the Memory Biology laboratory for helpful comments, discussions, and constructive suggestions. We thank the KAIST Bio-Core Center and the KAIST Analysis Center for Research Advancement (KARA) for use of confocal microscopes and assistance in performing imaging experiments.

Funding: This work was supported by grants from the National Research Foundation of Korea (NRF-2022M3E5E8081183 and NRF-2017M3C7A1031322).

Author contributions:

Conceptualization: J.H., J-H.H.
Data curation: J.H., J-H.H.
Formal analysis: J.H., B.S., J-H.H.
Funding acquisition: J-H.H.
Investigation: J.H., B.S.
Methodology: J.H., J-H.H.
Project administration: J-H.H.
Resources: J-H.H.
Software: J.H.
Supervision: J-H.H.
Validation: J.H., B.S., J-H.H.
Visualization: J.H., J-H.H.
Writing—original draft: J.H., J-H.H.
Writing—review & editing: J.H., B.S., J-H.H.

Competing interests:

Authors declare that they have no competing interests.

Data and materials availability:

All data needed to evaluate the conclusions in the paper are present in the paper and/or the Supplementary Materials.

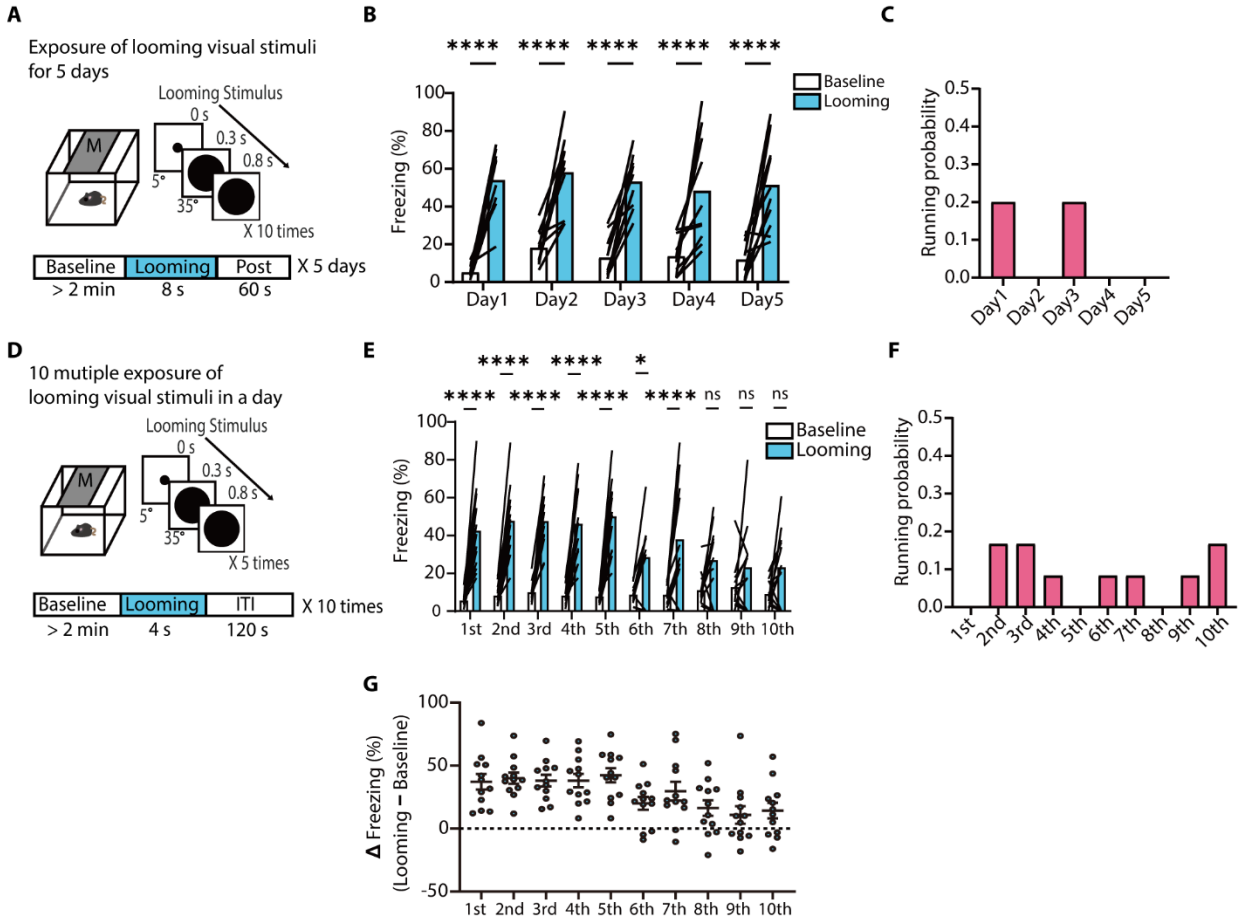

Fig. S1. CGRP^{PBN} neuronal activity in response to flickering and looming visual stimuli (related to Figure 1).

(**A**) Schematic of repeated behavioral tests for innate defensive responses to looming visual stimuli over 5 days. Each day, mice were exposed to 10 consecutive looming stimuli (8 s per trial).
(**B**) No significant habituation to daily looming stimuli over 5 days. Freezing responses to looming stimuli remained consistent (N = 10 mice; RM two-way ANOVA, Stimulus, $F_{1,18}$= 72.07, P< 0.0001).
(**C**) Probability of running responses to daily looming stimuli over 5 days, calculated as the number of mice exhibiting running behavior divided by the total number of mice.
(**D**) Schematic of a behavioral test for habituation of the innate freezing response to looming stimuli. A set of 5 looming stimuli (4 s each) was repeated 10 times with a 120-s intertrial interval.
(**E**) Habituation of innate freezing response. Freezing was measured during each 4-s looming stimuli (N = 12 mice; RM two-way ANOVA, Trials × Stimulus, $F_{9,198}$= 4.198, P< 0.0001).
(**F**) Probability of running event to the 10-repeated looming stimuli.
(**G**) Difference in freezing levels between baseline and looming stimuli (RM one-way ANOVA, $F_{9,99}$= 4.598, P< 0.0001).
All data are presented as mean ± s.e.m. *p < 0.05, ****p < 0.0001. ns, not significant.

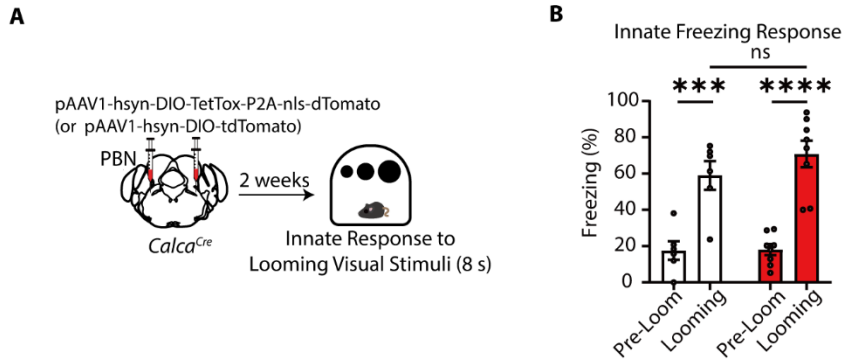

Fig. S2. TetTox inhibition of CGRP^{PBN} neurons did not impair innate defensive behavioral responses to looming visual stimuli (related to Figure 3).

(**A**) Schematic of innate freezing response test with TetTox-mediated inhibition of CGRP^{PBN} neurons.
(**B**) TetTox inhibition of the CGRP^{PBN} neurons did not affect innate freezing response to looming visual stimuli (tdTomato group, N= 6 mice; TetTox group, N= 8 mice; RM two-way ANOVA, Time, $F_{1,12}$= 68.01, P< 0.0001).
All data are mean ± s.e.m. ***p < 0.001, ****p < 0.0001. ns, not significant.

1311

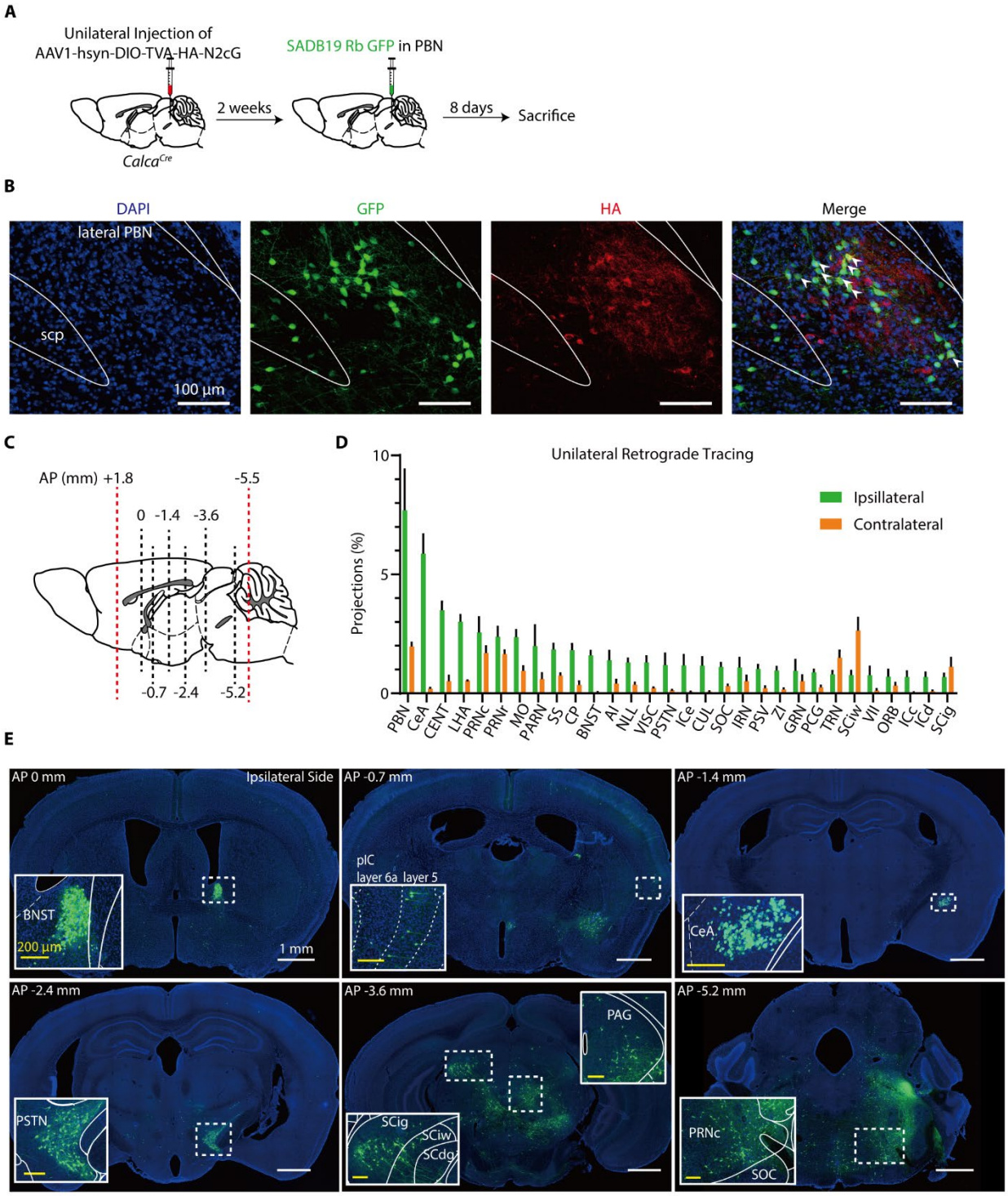
A
Unilateral Injection of
AAV1-hsyn-DIO-TVA-HA-N2cG
SADB19 Rb GFP in PBN
2 weeks
8 days
Sacrifice
Calca^Cre
B
DAPI
GFP
HA
Merge
lateral PBN
scp
100 µm
C
AP (mm) +1.8
-5.5
0 -1.4 -3.6
-0.7 -2.4 -5.2
D
Unilateral Retrograde Tracing
Ipsillateral
Contralateral
Projections (%)
10
5
0
PBN CeA CENT LHA PRNc PRNr MO PARN SS CP BNST AI NLL VISC PSTN ICe CUL SOC IRN PSV ZI GRN PCG TRN SCiw VII ORB ICc ICd SCig
E
AP 0 mm
Ipsilateral Side
BNST
200 µm
1 mm
AP -0.7 mm
pIC
layer 6a layer 5
AP -1.4 mm
CeA
AP -2.4 mm
PSTN
AP -3.6 mm
PAG
SCig
SCiw
SCdg
AP -5.2 mm
PRNc
SOC

1312

1313 **Fig. S3. Brain-wide monosynaptic retrograde tracing of CGPR^{PBN} neurons (related to**
1314 **Figure 4).**
1315 (**A**) Schematic of unilateral monosynaptic retrograde tracing of CGRP^{PBN} neurons. Unilateral
1316 injections of AAV2/1-hsyn-DIO-TVA-HA-N2cG into the PBN of *Calca*^{Cre} mice were followed
1317 by unilateral injections of SADB19-GFP rabies virus into the same site 2 weeks later.
1318 (**B**) Representative confocal microscopic images of coronal sections showing neurons expressing
1319 GFP and/or haemagglutinin (HA) tag in the PBN. White arrows indicate double-labeled starter
1320 cells (GFP+ & HA+). Scale bar, 100 µm.
1321 (**C**) AP range of coronal sections collected for imaging analysis (AP, +1.8 mm to -5.5 mm,
1322 indicated by dotted red lines) and AP coordinates of representative images shown in (E) (dotted
1323 black lines).
1324 (**D**) Distribution of retrogradely labeled neurons across the top 30 brain regions with the highest
1325 number of projections.
1326 (**E**) Representative images of coronal sections showing GFP-labeled retrogradely traced neurons
1327 in each analyzed target region. Insets show magnified views of the dotted boxes. Scale bars: 1
1328 mm (white bar) and 200 µm (yellow bar in insets).
1329
1330 **Abbreviations**: Agranular insular area (AI); Bed nuclei of the stria terminalis (BNST);
1331 Caudoputamen (CP); Central amygdalar nucleus (CeA); Central lobule (CENT); Culmen (CUL);
1332 Facial motor nucleus (VII); Gigantocellular reticular nucleus (GRN); Inferior colliculus, central
1333 nucleus (ICc); Inferior colliculus, dorsal nucleus (ICd); Inferior colliculus, external nucleus (ICe);
1334 Intermediate reticular nucleus (IRN); Lateral hypothalamic area (LHA); Nucleus of the lateral
1335 lemniscus (NLL); Orbital area (ORB); Parabrachial nucleus (PBN); Parvicellular reticular nucleus
1336 (PARN); Parasubthalamic nucleus (PSTN); Pontine central gray (PCG); Pontine reticular nucleus,
1337 caudal part (PRNc); Pontine reticular nucleus (PRNr); Principal sensory nucleus of the trigeminal
1338 (PSV); Somatomotor areas (MO); Somatosensory areas (SS); Superior colliculus, motor related,
1339 intermediate gray layer (Scig); Superior colliculus, motor related, intermediate white layer (Sciw);
1340 Superior olivary complex (SOC); Tegmental reticular nucleus (TRN); Visceral area (VIS); Zona
1341 incerta (ZI).
1342

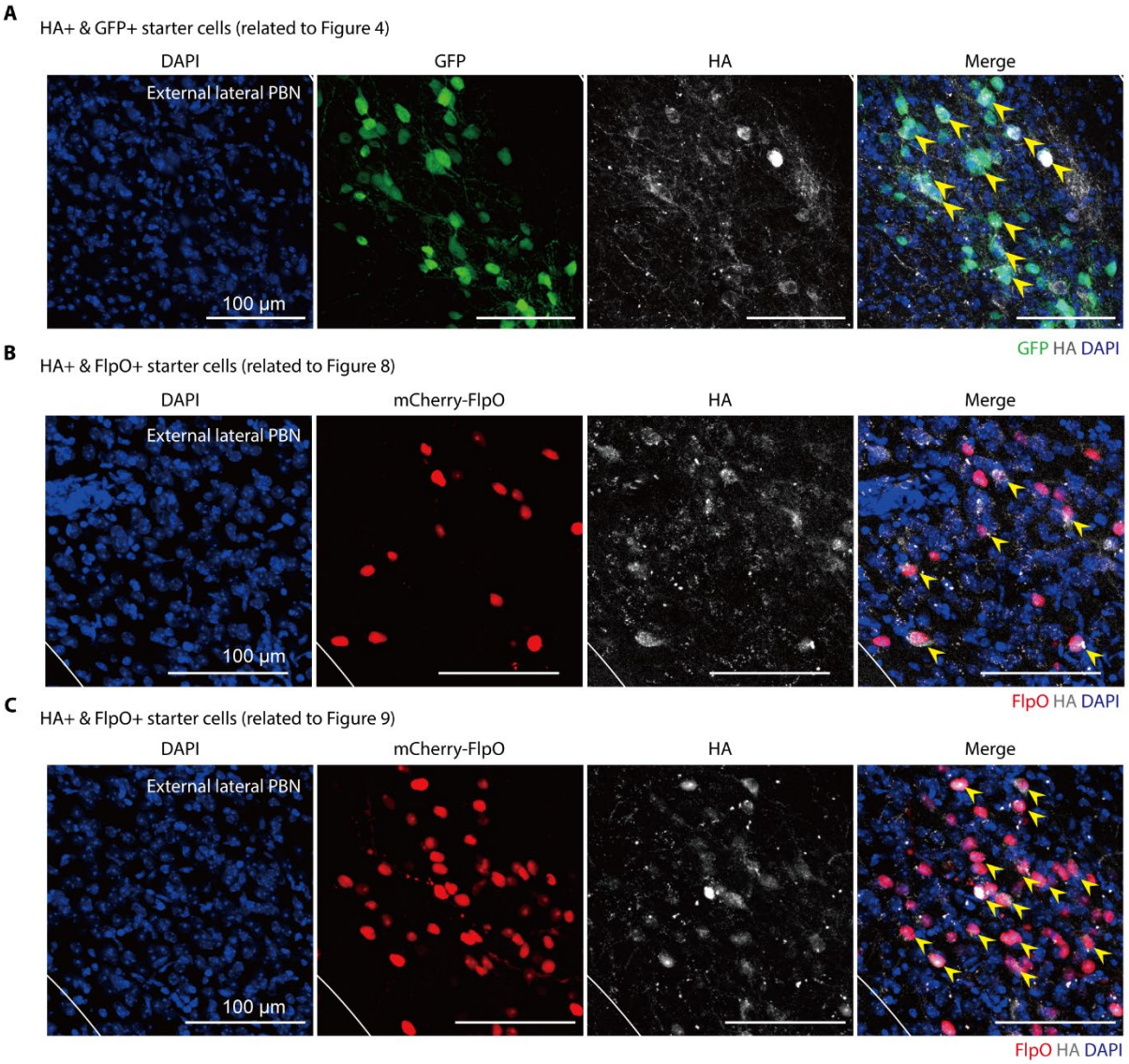

Fig. S4. Images of starter cells in the PBN in the monosynaptic retrograde labelling experiments (related to Figure 4, 8, and 9).

(**A**) Representative confocal microscopic images of coronal sections showing the neurons double-labeled for GFP and HA tag in the PBN. Yellow arrow head indicates double-labeled starter cells (GFP+ & HA+) in Figure 4.

(**B, C**) Representative confocal microscopic images of coronal sections showing the neurons expressing FlpO fused with mCherry and HA tag in the PBN, related to the experiments in Figure 8 (B) and Figure 9 (C). Yellow arrow head indicates double positive starter cells (mCherry-FlpO+ & HA+). Scale bars, 100 µm.

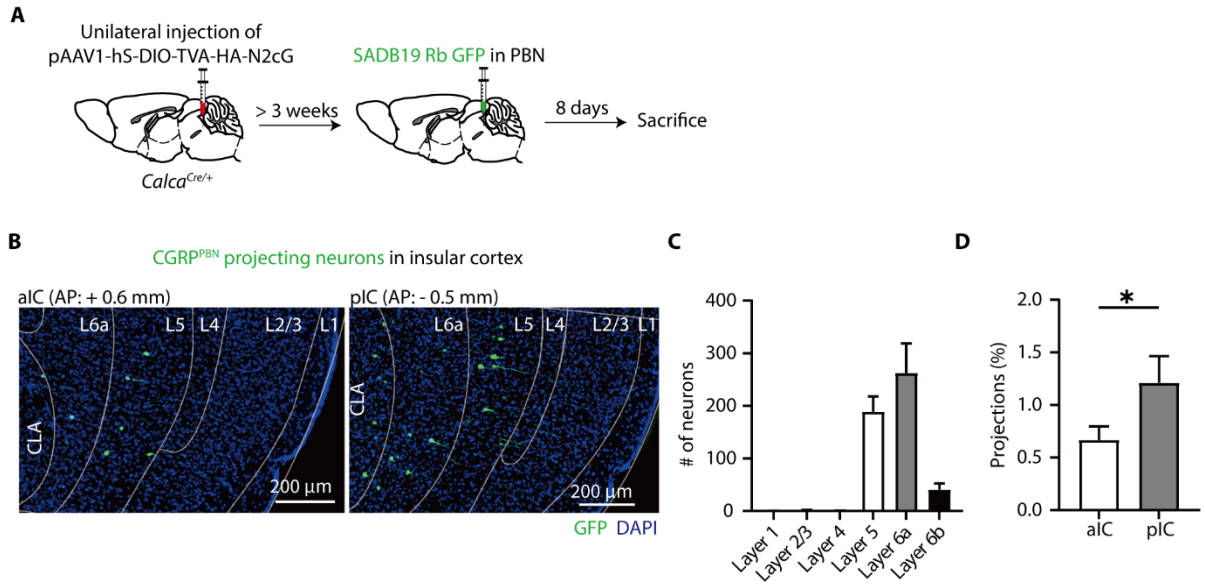

Fig. S5. Monosynaptic retrograde tracing of CGPR^{PBN} neurons in the insular cortex (related to Figure 4).

(A) Schematic of unilateral monosynaptic retrograde tracing of CGRP^{PBN} neurons.

(B) Representative images of coronal brain sections showing retrogradely labeled neurons with GFP in the anterior (left) and posterior (right) parts of the insular cortex.

(C) CGRP^{PBN}-projecting posterior insular neurons are specifically located in layers 5 and 6.

(D) Percentage of projections in the anterior and posterior insular cortex (N= 6 mice; Two-tailed paired t-test, t_5= 2.815, P= 0.0373).

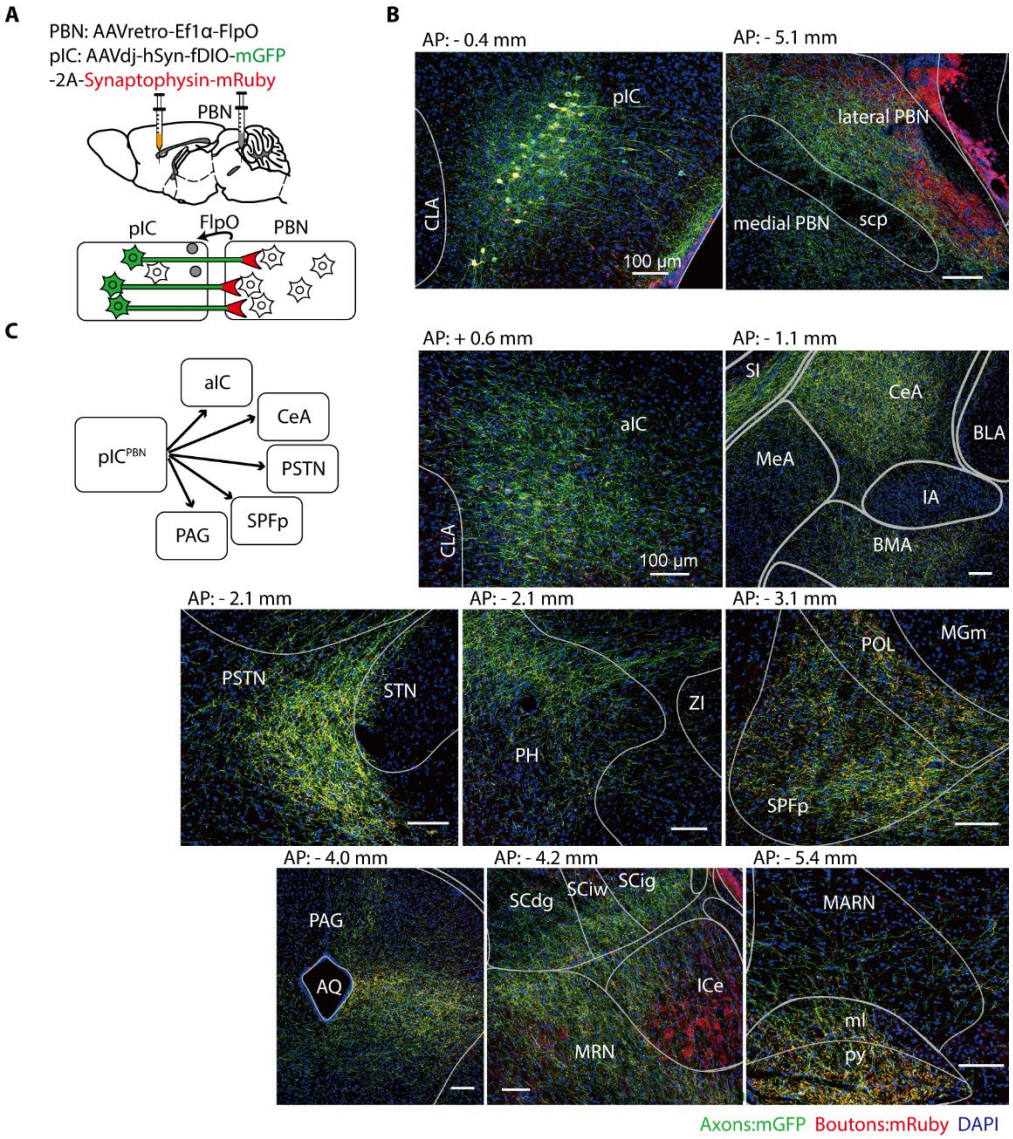

Fig. S6. Axon tracing of pIC$^{\rightarrow PBN}$ neurons (related to Figure 6).
(A) Schematic of unilateral axon tracing of pIC$^{\rightarrow PBN}$ neurons. Unilateral injections of AAVretro-EF1α-flpO into the PBN and AAVdj-hSyn-FLEX-mGFP-2A-Synaptophysin-mRuby into the pIC.
(**B**) Representative images of pIC$^{\rightarrow PBN}$ neurons (left) and projections to the PBN (right). Scale bars, 100 µm.
(**C**) Representative confocal microscopic images of coronal sections showing the axons (mGFP +) and synaptic bouton (mRuby +). Scale bars, 100 µm.

Abbreviations: Anterior insular cortex (aIC); Basolateral amygdalar nucleus (BLA); Basomedial amygdalar nucleus (BMA); Central amygdalar nucleus (CeA); Cerebral aqueduct (AQ); Claustrum (CLA); Inferior colliculus, external nucleus (ICe); Intercalated amygdalar nucleus (IA); Magnocellular reticular nucleus (MARN); Medial amygdalar nucleus (MeA); Medial geniculate nucleus, medial part (MGm); Medial lemniscus (ml); Midbrain reticular nucleus (MRN); Parasubthalamic nucleus (PSTN); Periaqueductal gray (PAG); Posterior hypothalamic nucleus (PH); Posterior insular cortex (pIC); Posterior limiting nucleus of the thalamus (POL); Pyramid (py); Subparafascicular nucleus, parvicellular part (SPFp); Substantia innominata (SI); Subthalamic nucleus (STN); Superior cerebellar peduncle (scp); Superior colliculus, deep gray

layer (SCdg); Superior colliculus, intermediate gray layer (SCig); Superior colliculus, intermediate white layer (SCiw); Zona incerta (ZI).